Genomics 115 (2023) 110731

Contents lists available at ScienceDirect

Genomics

journal homepage: www.elsevier.com/locate/ygeno

Deficiency of ligase IV leads to reduced NHEJ, accumulation of DNA damage, and can sensitize cells to cancer therapeutics

Nitu Kumari, Himanshu Antil, Susmita Kumari, Sathees C. Raghavan *

Department of Biochemistry, Indian Institute of Science, Bangalore 560012, India

ARTICLE INFO

Keywords:
Double-strand breaks
NHEJ
MMEJ
Cancer therapy
DNA repair
Nonhomologous DNA end joining
Microhomology mediated end joining

ABSTRACT

Ligase IV is a key enzyme involved during DNA double-strand breaks (DSBs) repair through nonhomologous end joining (NHEJ). However, in contrast to Ligase IV deficient mouse cells, which are embryonic lethal, Ligase IV deficient human cells, including pre-B cells, are viable. Using CRISPR-Cas9 mediated genome editing, we have generated six different LIG4 mutants in cervical cancer and normal kidney epithelial cell lines. While the LIG4 mutant cells showed a significant reduction in NHEJ, joining mediated through microhomology-mediated end joining (MMEJ) and homologous recombination (HR) were significantly high. The reduced NHEJ joining activity was restored by adding purified Ligase IV/XRCC4. Accumulation of DSBs and reduced cell viability were observed in LIG4 mutant cells. LIG4 mutant cells exhibited enhanced sensitivity towards DSB-inducing agents such as ionizing radiation (IR) and etoposide. More importantly, the LIG4 mutant of cervical cancer cells showed increased sensitivity towards FDA approved drugs such as Carboplatin, Cisplatin, Paclitaxel, Doxorubicin, and Bleomycin used for cervical cancer treatment. These drugs, in combination with IR showed enhanced cancer cell death in the background of LIG4 gene mutation. Thus, our study reveals that mutation in LIG4 results in compromised NHEJ, leading to sensitization of cervical cancer cells towards currently used cancer therapeutics.

1. Introduction

The DNA in our cells is under constant assault from various exogenous and endogenous sources. Failure to maintain genomic integrity can lead to mutations, chromosomal aberrations, translocations, and carcinogenesis [1–3]. To ensure error-free and faithful transmission of hereditary material, human cells employ several DNA repair pathways to repair each type of DNA damage [4]. DNA double-strand breaks (DSBs) are the most lethal among all the DNA damages, and can be generated either by exogenous sources like radiation, radiomimetic agents, genotoxic chemicals, or endogenous sources such as reactive oxygen species (ROS), inadvertent enzymatic activity and replication fork arrest [5,6]. DSBs are majorly repaired by either of the two repair pathways, namely homologous recombination (HR) and nonhomologous end joining (NHEJ) [7–10]. HR requires genetic information from the homologous DNA sequence of the partner chromosome for repair, whereas NHEJ (also called classical NHEJ or cNHEJ) involves the direct end-to-end joining of the broken ends. Enzymatic requirements of these pathways are well defined [6,8,10,11]. Much later, another DSB repair pathway was identified, which is operational in the absence of cNHEJ factors known as microhomology-mediated end joining (MMEJ) [12,13].

During NHEJ, KU70/KU80 heterodimer recognizes DSBs and binds to the broken DNA. KU70/KU80 prevents the DNA from further resection and acts as scaffold to which other NHEJ proteins are recruited for the completion of NHEJ [8]. DNA-dependent protein kinase catalytic subunit (DNA-PKcs) binds to KU with DNA and forms the DNA-PK complex [8,14,15]. DNA-PKcs undergoes autophosphorylation and activates the Artemis endonuclease leading to cleavage of 5′ and 3′ overhang [16,17]. After DNA end processing, the gap is filled by DNA pol X family polymerases (μ and λ) generating ends that can be efficiently ligated [18,19]. Finally, the nick is sealed by the DNA Ligase IV-XRCC4-XLF complex, restoring intact DNA [20,21]. PAXX (Paralogue of XRCC4 and XLF) is a recently discovered protein, which helps in stabilization of the NHEJ machinery [22]. Finally, in case of DNA polymerase μ mediated NHEJ, RNase H2 is involved in the removal of rNMP incorporated by Pol μ [23,24]. DSBs generated during programmed V(*D*)J recombination is also repaired by NHEJ and in this process terminal deoxynucleotidyl transferase (TdT) polymerase adds nucleotide in template independent manner and nick is sealed by Ligase IV/XRCC4 [8,25,26].

There are three different DNA ligases in human cells, Ligase I, Ligase

* Corresponding author.
E-mail address: sathees@iisc.ac.in (S.C. Raghavan).

https://doi.org/10.1016/j.ygeno.2023.110731
Received 11 April 2023; Received in revised form 14 September 2023; Accepted 19 October 2023
Available online 21 October 2023

III and Ligase IV [11,27]. Ligase I is involved in sealing of Okazaki fragments during DNA replication and also participates in base excision repair (BER) [28]. Ligase III plays a major role in short-patch BER and single-strand breaks repair in the nucleus and it is also important for the maintenance of mitochondrial DNA [29–31]. Ligase I and Ligase III are also involved in MMEJ or Alt-NHEJ repair pathway [12,30,32], whereas DNA Ligase IV is the critical component of NHEJ and V(*D*)J recombination [33].

Despite some functional overlap between all the three ligases, transgenic knockout (KO) mouse models of Ligase III and Ligase IV are embryonic lethal and Ligase I is required for normal development hence all the three ligases are essential for survival [34–36]. DNA Ligase IV is a 911 amino acid long protein encoded by the gene LIG4 and located on human chromosome 13 [37]. DNA Ligase IV contains C-terminal tandem repeat of BRCT domains, which is unique to Ligase IV and is responsible for its function during NHEJ which cannot be replaced by other mammalian ligases [31]. However, the N-terminal catalytic domain of DNA Ligase IV comprised of three subdomains- the DNA-binding (DBD), nucleotidyltransferase (NTD), and oligonucleotide/oligosaccharide-fold (OBD) subdomains shares homology with DNA Ligase I and Ligase III [38].

Disruptions in DNA repair genes due to mutations has been linked with cancer progression [9,39–41]. Among NHEJ repair proteins, DNA-PKcs and KU proteins have been shown to be upregulated in breast cancer, gastric cancer, oral squamous cell carcinoma, oesophageal cancer, and lung cancer [9,42]. Compared to the normal cells, Ligase IV and XRCC4 showed elevated expression in a pan cancer manner [42]. Ligase IV and XRCC4 polymorphisms have also been reported in breast cancers [43]. Interestingly, a recent study of whole-exome sequencing from cervical carcinomas showed mutations in LIG4 gene of four patients [44]. Apart from this, several hypomorphic DNA Ligase IV mutations have been identified which are responsible for LIG4 syndrome [45]. Moreover, there is a lack of reports for Ligase IV null mutations suggesting that such a mutant might be nonviable in humans. The clinical symptoms of functionally deficient DNA Ligase IV patients include, microcephaly, skin abnormalities, radiosensitivity, growth, and developmental deficiencies, and immunodeficiency [46,47]. The mutations observed in the Ligase IV are R278H, Q280R and H282L, positioned close to the active catalytic site K273 of the conserved ligase motif and therefore result into 5–10% residual adenylation and dsDNA joining activity [46]. Two common mutations/polymorphisms, A3V and T9I have also been reported in the N-terminus of Ligase IV [46]. Other mutations associated with Ligase IV syndrome are Q280 and H282 on β3 and Y288 on β4 within the core of NTD and these mutations mostly alters the β-sheet structure and hence ATP-binding pocket [48]. Small molecule inhibitors of Ligase IV such as L189, SCR7, SCR130, SCR116, SCR132 have been developed recently [9,49–52]. Several such NHEJ inhibitors have showed elevated radio and chemo sensitivity against cancer [53,54].

180BR is a first cell line derived from defective Ligase IV-patient, which showed radiosensitivity and defects in DSB repair, however, they were able to carry out V(*D*)J recombination [55,56]. Later the homozygous mutation in 180BR cell line was identified as R278H substitution and is responsible for the radiosensitivity of the cells [57,58]. Targeted deletion of DNA Ligase IV in human pre-B cell line showed defective V(*D*)J recombination activity [33], significant impairment in the joining efficiency and are required for the DNA end protection [59]. In another study, Ligase IV deficient DT40 chicken B-lymphocyte cell line has been shown to be more radiosensitive and no impairment in HR [60]. Till date, most of the studies related to Ligase IV deficient cell lines are mostly performed in lymphoid cells which limits our scope of understanding the role of Ligase IV in normal transformed cell line or any other cancer cell lines.

In the present study, we have generated several different mutants of DNA LIG4 in HeLa and HEK293T cell lines using CRISPR-Cas9 technology, characterized and explored the cellular response of LIG4 mutated cells towards different DNA damaging agents and cancer therapeutics. We report that the viability of LIG4 mutant cells is compromised due to slow repair of DSBs, leading to its accumulation. While the efficacy of NHEJ was significantly hampered in LIG4 mutant cells, an elevated DSB repair through MMEJ and HR was noted. Finally, we showed that LIG4 mutant cells are highly sensitive to DNAdamaging agents and chemotherapeutic drugs particularly, when used in combination with IR. Our findings could be used as a promising strategy to sensitize cancer cells with mutations in DSB repair genes.

2. Materials and methods

2.1. Oligomers

Oligomers used in the study are presented as Table 1.

2.2. Enzymes, chemicals, and reagents

Chemicals and reagents used for the experiments were purchased from Sigma-Aldrich (USA), and SRL (India). DNA modifying enzymes were purchased from New England Biolabs (USA). [γ-P^{32}] ATP was purchased from BRIT (Hyderabad, India). Cell culture medium and PenStrep were from Lonza (Switzerland). Fetal bovine serum was bought from Gibco (USA). Antibodies were obtained from Santa Cruz (USA), and Sigma-Aldrich (USA).

2.3. Mammalian cell culture

Human cell lines HEK293T (human embryonic kidney cells) and HeLa (human cervical cancer) were purchased from National Centre for Cell Science, Pune, India. Cells were grown in DMEM supplemented with 10% FBS and 100 μg/ml Penicillin G and Streptomycin. Cells were incubated at 37°C in a humidified atmosphere containing 5% CO_2.

2.4. Plasmids and bacterial strains

The LentiCRISPRv2 plasmid was a gift from Feng Zhang, USA (Addgene plasmid # 52961; http://n2t.net/addgene:52961). The *in vivo* NHEJ construct pim-EJ5GFP was a gift from Dr. Jeremy Stark, USA. I-*Sce*I overexpression vector was obtained from Dr. Ralph Scully, USA. *E. coli* Rosetta(DE3)pLysS cells were purchased from Novagen (USA). The dual expression plasmid with Ligase IV and XRCC4 (pMJ4052) was a kind gift from Dr. Mauro Modesti (France). Overexpression construct, pMS13 was previously generated in-house [51]. The HR assay plasmids, pTO223 and pTO231 were from Dr. Christian Sengstag, Switzerland [61].

2.5. 5′ end-labelling of oligomeric DNA and annealing

5′-end labelling of oligomeric DNA was carried out using T4 polynucleotide kinase (NEB) in a buffer containing 20 mM Tris-acetate (pH 7.9), 10 mM magnesium acetate, 50 mM potassium acetate, 1 mM dithiothreitol (DTT), and [γ-P^{32}] ATP for 1 h at 37 °C. The labelled substrates were purified as described earlier [62–64] and stored at −20°C until further use. The double stranded substrates were prepared by annealing γ-P^{32}-labelled top strand (SCR19) oligomer with cold bottom strand oligomer (SCR20) in a ratio of 1:3 in the presence of 100 mM NaCl and 1 mM EDTA in a boiling water bath for 10 min followed by slow cooling as described earlier [64,65].

2.6. Design of single guide RNAs (sgRNAs) and construction of plasmid for CRISPR-Cas9 mediated knockout of LIG4 gene

Single guide RNAs (sgRNA) were designed and cloned as described earlier [66,67]. Briefly, sgRNA1 was constructed to target nucleotide position 2424 and sgRNA2 to target nucleotide position 915 of the

Table 1
List of oligomers used in the study.

Name	Nucleotide sequence
SCR19	5'-GATCCCTCTAGATATCGGGCCCTCGATCCGGTACTACTCGAGCCGGCTAGCTTCGA-TGCTGCAGTCTAGCCTGAG-3'
SCR20	5'-GATCCTCAGGCTAGACTGCAGCATCGAAGCTAGCCGGCTCGAGTAGTACCGGATC-GAGGGCCCGATATCTAGAGG-3'
SS54	5'-GATTAGATAATCAGTTCATCGAGTCCTCACGTAGATCGGTACTACTCGAGCTGAG-3'
SS62	5'TTAACTCAGCTCGAGTAGTACCGATCTACGTGAGGACTCGATGAACTGATTATCT-3'
SS65	5'-AGCTAACTGCATCTGTAGGTCGCGAATCAGTTCACTGCTTAA-3'
SS66	5'-GCAGTGAACTGATTCGCGACCTACAGATGCAGTT-3'
SS60	5'-AACTGCATCTGTAGGTCG-3′
SS61	5'-GAGTAGTACCGATCTACGTG−3'
NK24	5'-CACCGTGGCGTCGAAACATACTGAG-3′
NK25	5'-AAACCTCAGTATGTTTCGACGCCAC-3'
NK26	5'-CACCGGGGGTAAGAGAACCTTCAGT-3'
NK27	5'-AAACACTGAAGGTTCTCTTACCCCC-3'

available cDNA sequence of human DNA Ligase IV (Fig. 1A). sgRNA1 (NK24/NK25) and sgRNA2 (NK26/NK27) were synthesized with overhangs complementary to the *Bsm*BI digested site, annealed and cloned into LentiCRISPRv2 backbone at BsmBI restriction enzyme site using T4 DNA ligase. Identity of the plasmid constructs with sgRNA1 (pNK1) and sgRNA2 (pNK2) were confirmed by DNA sequencing. HeLa and HEK293T cells were transfected with the constructs containing sgRNA1 and sgRNA2 (pNK1 and pNK2) using branched PEI (DNA:PEI = 1:2) and incubated at 37°C. After 72 h, medium was changed and cells were incubated in DMEM medium containing 0.5 μg/ml puromycin for 3 weeks. Two wells of HeLa and four wells of HEK293T showed proliferation in medium containing puromycin after multiple rounds of puromycin selection. Genomic DNA was isolated from these puromycin resistant cells, PCR amplified, cloned into TA vector, and subjected to DNA sequencing. Sequencing analysis confirmed the presence of mutations near catalytic domain of Ligase IV (Fig. 1F).

2.7. Immunoblotting

To check the expression of Ligase IV in mutant cells, ~30 μg of each extract from wild type (WT) and LIG4 mutant cells were loaded on 8% SDS-PAGE and after electrophoresis, transferred to PVDF membrane [12,68–70]. The membrane was stained with ponceau S (as a loading control) and then blocked with 5% skim milk (in PBST). Blots were washed with PBST and incubated overnight with respective primary antibodies against Ligase IV (1:2000, Sigma) and PCNA (1:1000, Santa Cruz). Blots were washed with PBST and then incubated for 4 h with HRP-conjugated respective secondary antibodies (1:5000). Blots were developed using chemiluminescent substrate (Millipore) and images were captured using a LAS4000 chemi-detection system.

2.8. Preparation of cell-free extract

Cell-free extract (CFE) was prepared from WT and LIG4 mutant HeLa and HEK293T cells as described previously [62,69,71–74]. Approximately, 10^8 cells were resuspended in 2 volume of hypotonic buffer (10 mM Tris-HCl [pH 8.0], 1 mM EDTA, 5 mM DTT and protease inhibitors) and homogenized and incubated at 4 °C for 20 min. After that, half volume of high-salt buffer (50 mM Tris-HCl [pH 7.5], 1 M KCl, 2 mM EDTA and 2 mM DTT) was added, homogenized and incubated on ice for 20 min. Extracts were ultracentrifuged at 4 °C for 3 h at 42,000 RPM in a TLA-100 rotor. Supernatant was collected and dialyzed overnight against dialysis buffer (20 mM Tris-HCl (pH 8.0), 0.1 M potassium acetate, 20% *v*/v glycerol, 0.5 mM EDTA, 1 mM DTT and 0.1 mM PMSF). Extracts were aliquoted and stored at −80°C until use.

In vitro NHEJ assay was performed as described earlier with modifications [51,62,74]. We incubated 4 nM radiolabelled oligomeric DNA with optimum amount of CFEs in buffer containing 30 mM HEPES-KOH (pH 7.9), 7.5 mM $MgCl_2$, 1 mM DTT, 2 mM ATP, 50 μM dNTPs and 0.1 μg of bovine serum albumin in a reaction volume of 10 μl for 1 h at 30°C. Joining reaction was terminated by adding 10 mM EDTA and DNA was purified by phenol-chloroform extraction, followed by ethanol precipitation in presence of glycogen. The pellet was resuspended in 10 μl of TE and resolved on 8% denaturing PAGE, which was then dried and exposed. The signals were detected using phosphorImager (GE life sciences, USA) and analyzed with Multi Gauge (V3.0) software. Multi Gauge (V3.0) software was used for the quantification of bands of interest. The intensity (in photo-stimulated luminescence (PSL)/mm^2 units) obtained from each lane was plotted and presented as a bar diagram. GraphPad Prism (V5) software was used for statistical analysis.

Reconstitution NHEJ experiment was performed by adding 0.5 μg of purified Ligase IV/XRCC4 protein along with CFEs from LIG4 mutant HeLa KO1 and HEK293T KO3 cells. Reaction was incubated in a reaction volume of 10 μl for 1 h at 30 °C and processed further as described above.

2.9. NHEJ reporter assay

Intracellular NHEJ activity was measured as described previously [51,75,76]. Briefly, wild type (WT) and LIG4 mutant cells of HeLa and HEK293T (3×10^5) were seeded in 6 well plates and transfected with 20 μg of I-*Sce*I overexpression construct and 15 μg of pimEJ5-GFP reporter construct using branched PEI and incubated at 37 °C. After 36 h cells were harvested and the number of GFP positive cells were analyzed by Flow cytometry (Cytoflex S, Beckman Coulter, USA). pcDNA3.1-RFP was used as a transfection control and bar graph was plotted for percentage of GFP positive cells following normalization of transfection efficiency.

2.10. MMEJ assay

For MMEJ assay, DNA substrates containing 10 nt microhomology were prepared by annealing DNA oligomer SS54 with SS62 and SS65 with SS66. 4 nM of each DNA substrate was incubated with 2 μg of cell-free extracts from HeLa and HEK293T WT and LIG4 mutant cells in MMEJ buffer (10 mM Tris-HCl [pH 8.0], 20 mM $MgCl_2$, 1 mM ATP, and 1 mM DTT) in a reaction volume of 20 μl at 37 °C for 30 min [12,30,77]. Reaction was stopped by heat inactivation at 65 °C for 20 min. Joined products were detected by PCR using (γ-^{32}P) ATP-labelled primer, SS60 and unlabeled primer SS61 [denaturation: 95 °C for 3 min (1 cycle); denaturation: 95 °C for 30 s, annealing: 58 °C for 30 s, extension: 72 °C for 30 s (15 cycles); extension: 72 °C for 3 min (1 cycle)]. Joined products were resolved on 10% denaturing polyacrylamide gel, dried and then exposed. A 60 nt radiolabelled oligomer was used as marker. The signals were detected using phosphorImager (Fuji, Japan) and analyzed with Multi Gauge (V3.0) software.

2.11. HR assay

HR assay was performed as described earlier [61,74,78–80]. HR reaction was done by incubating HeLa and HEK293T wild type and LIG4 mutant (HeLa KO1 and HEK293T KO3) cell-free extract with plasmids,

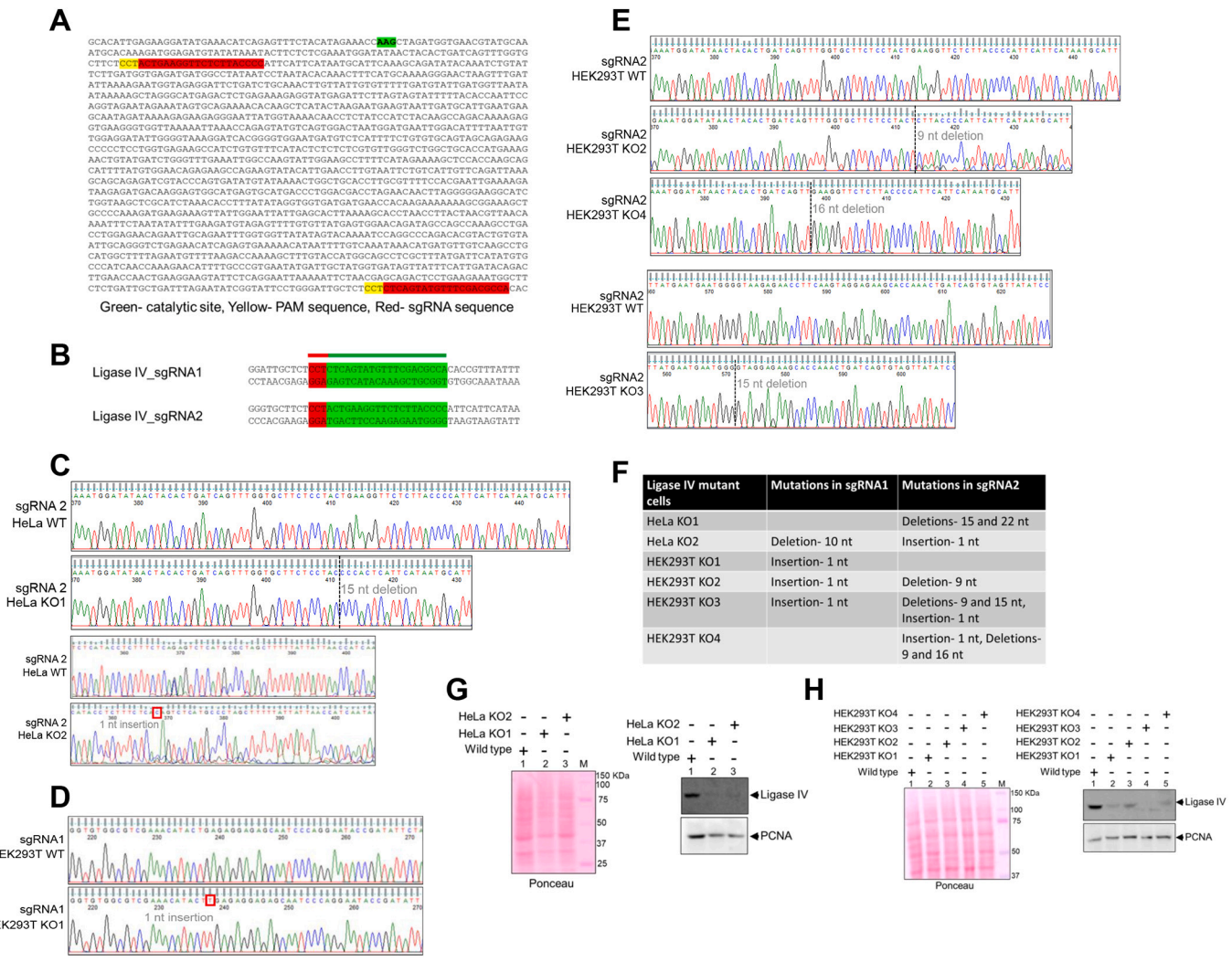

Ligase IV mutant cells	Mutations in sgRNA1	Mutations in sgRNA2
HeLa KO1		Deletions- 15 and 22 nt
HeLa KO2	Deletion- 10 nt	Insertion- 1 nt
HEK293T KO1	Insertion- 1 nt	
HEK293T KO2	Insertion- 1 nt	Deletion- 9 nt
HEK293T KO3	Insertion- 1 nt	Deletions- 9 and 15 nt, Insertion- 1 nt
HEK293T KO4		Insertion- 1 nt, Deletions- 9 and 16 nt

Fig. 1. Generation of LIG4 mutant cells and evaluation of Ligase IV expression following introduction of mutation in LIG4 gene. A. Position of sgRNA1 and sgRNA2 in the CDS of exon 2 of LIG4 gene. While sgRNA1 is designed against BRCT2 domain, sgRNA2 is designed against NTD domain. Red colour indicates the position of sgRNA1 (bottom, nucleotide position 2424 of exon 2) and sgRNA2 (top, nucleotide position 915 of exon 2), yellow colour indicates the PAM site and green colour indicates the catalytic site of Ligase IV enzyme. B. Sequence of the sgRNA1 and sgRNA2 used for gene editing of human LIG4. Green colour indicates the sgRNA sequence and red colour shows the PAM site sequence. The sgRNA encoding oligomers containing *Bsm*BI digested overhangs were cloned into the LentiCRISPRv2 backbone to generate the sgRNA constructs (pNK1 and pNK2). C-E. Representative chromatogram from each LIG4 mutant cell line showing the presence of insertion/deletions (Black dotted line indicates deletions and insertion is highlighted in red box) in the LIG4 gene of the mutant cell lines. Representative chromatogram for mutations in sgRNA2 sequence of HeLa KO1 (HeLa.Lig4.catDΔ.1.NK) and HeLa KO2 (HeLa.Lig4.catDΔ.2.NK) (C), for insertion in sgRNA1 sequence for HEK293T KO1 (HEK293T.Lig4.catDΔ.1.NK) (D), and for mutations in HEK293T KO2 (HEK293T.Lig4.catDΔ.2.NK), HEK293T KO3 (HEK293T.Lig4.catDΔ.3.NK), and HEK293T KO4 (HEK293T.Lig4.catDΔ.4.NK) (E) are shown. Only one representative chromatogram is shown for each case. F. Table showing summary of different types of mutations (insertion and deletions) present at or near sgRNA1 and sgRNA2 in the LIG4 gene of HeLa and HEK293T LIG4 mutant cells. G. Western blot analysis showing the level of Ligase IV protein expression in the WT and the LIG4 mutant HeLa cells. PCNA served as loading control. H. Western blot analysis showing the level of Ligase IV expression in the WT and the LIG4 mutant HEK293T cells. Ponceau-stained blot and PCNA served as loading control. (For interpretation of the references to colour in this figure legend, the reader is referred to the web version of this article.)

pTO223 (500 ng) and pTO231 (500 ng). The reaction was carried out by incubating cell-free extracts (1 μg) in HR buffer containing 35 mM of HEPES (pH 7.9), 10 mM of $MgCl_2$, 1 mM of DTT, 1 mM of ATP, 50 μM of dNTPs, 1 mM of NAD and 100 μg/ml of BSA in a volume of 25 μl at 37 °C (30 min). The reactions were terminated by adding EDTA (20 mM), proteinase K (200 μg/ml), and SDS (0.5%) followed by product purification by phenol/chloroform extraction and precipitation. The purified DNA was resuspended in TE (20 μl) and 2 μl of it was used for transformation into electro-competent *Escherichia coli* DH5α. The transformed bacterial cells were plated either on ampicillin or ampicillin-kanamycin plates to score the transformants and recombinants, respectively. The recombination frequency was calculated as the ratio of the number of recombinants to the number of transformants obtained per microgram of DNA.

The plasmid DNA was isolated from the recombinant clones, after growing in 2 ml of LB broth at 37 °C (for 14 h) as per standard protocol [81]. Plasmid DNA (~1 μg) was then subjected to restriction enzyme digestion using *Eco*RI/*Sal*I at 37 °C (for 3 h). Restriction digestion of pTO223 and pTO231 with EcoRI/SalI would release 1.25 and 1.2 kb fragments, respectively, showing neo*Δ2* and *neoΔ1* allele and a 2.9 kb fragment corresponding to vector DNA. In contrast, restriction digestion of plasmids containing functional *neo* gene will release a 1.5 kb fragment indicating the presence of functional *neo* gene. The digestion products were resolved on 1% agarose gel to confirm recombinants. Both plasmids with nonfunctional neomycin genes were also digested as controls.

2.12. Immunofluorescence (IF)

Immunofluorescence was performed as described previously [51,54,82–84]. For immunofluorescence, 2×10^5 cells were seeded on coverslip and allowed to adhere, harvested, washed with 1× PBS. For radiation treatment, cells were irradiated and allowed for appropriate time of recovery as mentioned in the figures, fixed with 2% paraformaldehyde for 10 min and permeabilized with PBST (1× PBS containing 0.1% Triton X-100) for 10 min, blocking with PBST containing 0.1% BSA and 10% FBS (1 h, 4 °C). After blocking, cells were incubated with anti- γ-H2AX (1:500, Cell Signaling Technology, USA) overnight at 4 °C, followed by Alexa Fluor-488 or 594 conjugated anti-mouse secondary antibody (1:100) for 2 h at room temperature. After washing with 1× PBS, coverslips were mounted using propidium iodide (PI)/DAPI and DABCO (antifade). Images were captured using confocal microscope (Olympus, FLUOVIEW FV3000, Japan) and the images were processed by Olympus Software. The number of γ-H2AX foci in each cell was counted and plotted as a scatter plot using GraphPad Prism 7.

For repair kinetics experiment wild type and LIG4 mutant cells were seeded on coverslip, allowed to adhere and irradiated with 2 Gy and recovery was investigated at different time points (30 min, 6 h and 18 h). After recovery, cells were harvested and processed for IF as described above.

2.13. Cell viability assay

Cell viability was measured by trypan blue exclusion assay. Cells were mixed with equal volume of 0.4% Trypan blue (Millipore Sigma) and counted using hemocytometer. The number of viable cells (not stained with Trypan blue) was plotted. Cell viability assay was repeated a minimum of four times for each cell line and plotted using GraphPad Prism 7. Cell viability was also measured using alamar blue assay [85]. For that 10,000 cells were seeded and incubated for 24, 48 and 72 h. At each time point, 1× alamar blue dye was added and incubated at 37 °C for 3–4 h and then absorbance was taken at wavelength of 570 nm and 600 nm using microplate reader (Tecan Infinite M200).

For the cytotoxicity assay using different FDA approved drugs Carboplatin, Paclitaxel, Doxorubicin, Cisplatin, Bleomycin, Azacytidine, 5-FU and mirin, HeLa WT and LIG4 mutant cells (2.5×10^4) were seeded. Different concentrations of drugs were added either alone or in combination with two drugs or in combination with IR. After 48 h of incubation at 37 °C, cell viability was measured by trypan blue exclusion assay.

Cells were treated with different compounds at 3 different concentrations, Carboplatin (10, 30 and 60 μM), Paclitaxel (1, 3 and 9 nM), Doxorubicin (0.1, 5 and 25 nM), Cisplatin (5, 15 and 30 μM), Bleomycin (5, 15 and 30 μM), Azacytidine (0.5, 1.5 and 4.5 μM), Mirin (20, 40 and 60 μM) and 5-FU (0.5, 1.5 and 4.5 μM). Cells were also treated in combinations with Cisplatin (2.5, 7.5 and 15 μM) and Carboplatin (0.5, 2.5 and 7.5 μM), Doxorubicin (0.01, 0.1 and 1 nM) and Cisplatin (2.5, 7.5 and 15 μM), Paclitaxel (0.005, 0.05 and 0.5 nM) and Cisplatin (2.5, 7.5 and 15 μM), Carboplatin (0.5, 2.5 and 7.5 μM) and Paclitaxel (0.005, 0.05 and 0.5 nM), Doxorubicin (0.01, 0.1 and 1 nM) and Paclitaxel (0.005, 0.05 and 0.5 nM), Doxorubicin (0.01, 0.1 and 1 nM) and Carboplatin (0.5, 2.5 and 7.5 μM). For cytotoxicity assay in presence of IR and drug combination, different drugs such as Cisplatin (0.5 μM), Doxorubicin (0.01 nM), Paclitaxel (0.01 nM), Bleomycin (5 μM), and Carboplatin (0.5 μM) were used with 0.5 Gy IR.

2.14. Irradiation

Cells were irradiated with 2 Gy at room temperature using a Cobalt-60 gamma irradiator (BI 2000, BRIT, India) [56,84,86]. The dose rate of the source at the time of usage was 0.61 Gy/min. Post irradiation, cells were incubated at 37 °C for specified time before harvesting the cells for further experiments. For combination experiments, cells were exposed to 0.5 Gy of IR.

2.15. Overexpression of Ligase IV in LIG4 mutant cells and exposure to IR

For overexpression, LIG4 mutant HeLa and HEK293T cells were seeded (3×10^5 cells). Transfection was performed by Polyethyleneimine (PEI) method, as described earlier [67,82,87]. Briefly, cells were transfected using branched PEI (DNA: PEI = 1:2) with Ligase IV overexpression construct (pMS13) and incubated at 37 °C and 5% CO_2 for 36 h. After that, cells were irradiated with 2 Gy and allowed to recover for 1 h followed by IF studies. IF was performed as described above.

2.16. Overexpression and purification of Ligase IV/XRCC4

The plasmid with His-tagged Ligase IV and XRCC4 was a kind gift from Dr. Mauro Modesti [88]. Rosetta(DE3)pLysS cells were transformed with the expression vector, grown to an $O{\cdot}D_{600}$ of 0.6 and then induced with 1 mM IPTG (16 h at 16°C). Protein was purified as described earlier [51,52,88]. Briefly, cells were harvested, extracts were prepared with the extraction buffer (20 mM Tris–HCl [pH 8.0], 0.5 M KCl, 20 mM imidazole [pH 7.0], 20 mM β-mercaptoethanol, 10% glycerol, 0.2% Tween 20, 1 mM PMSF) and loaded on Ni-NTA column as per manufacturer's instructions (Novagen, USA). Fractions were collected, purest fractions were pooled and reloaded on to UNO sphere Q anion exchange column (BioRad USA), following which the protein was eluted by gradient of KCl. Appropriate fractions were pooled, dialyzed (Dialysis buffer: 20 mM Tris-HCl [pH 8.0], 150 mM KCl, 2 mM DTT and 10% glycerol) and stored at 80 °C. The purity of the proteins was confirmed by SDS-PAGE (CBB stain).

2.17. Neutral comet assay

Neutral comet assay was performed as described previously [52,70]. HeLa and HEK293T WT and LIG4 mutant cells (25,000 cells/ml) were treated with 4 μM etoposide and incubated for 4 h. Cells were harvested and washed with 1× PBS, mixed in low melting agarose, spread on agarose-coated slides and lysed overnight in neutral lysis buffer (0.5 M EDTA, 2% Sarkosyl and 0.5 mg/ml Proteinase K) at 37 °C. Electrophoresis was carried out at 12 V for 25 min in neutral electrophoresis buffer (90 mM Tris HCl [pH 8], 90 mM Boric acid and 2 mM EDTA). Cells were stained with Propidium Iodide (2.5 μg/ml for 20 min) and imaged using Zeiss AxioVision (Germany) microscope. The experiment was repeated for 3 times and a minimum of 100 cells per sample were considered from each batch for analysis of olive moment using CometScore software and plotted using GraphPad Prism software.

2.18. Structure prediction using SWISS-MODEL

EXPASY Translate tool was used to predict the amino acid sequence of the polypeptide from mRNA of mutated Ligase IV cell lines (generated by CRISPR) [89]. The same sequence was used for homology modelling of the putative truncated Ligase IV protein. Homology modelling was performed using the crystal structure of Ligase IV as a template (PDB ID: 3W50) using SWISS-MODEL and textured in 3D builder [66].

2.19. Statistical analysis

Statistical analysis was carried out using GraphPad Prism. Significance was calculated using either Students' *t*-test or one-way ANOVA. The obtained values were considered significant if the p value was <0.05 and * denotes $p < 0.05$, ** denotes $p < 0.005$, and *** denotes $p < 0.0001$ respectively.

3. Results

3.1. Generation of LIG4 mutant of HeLa and HEK293T cells by CRISPR-Cas9 technology

CRISPR-Cas9 genome editing was used for the generation of Ligase IV knockout (KO) in HeLa (human cervical cancer) and HEK293T (human embryonic kidney epithelial cell) cells. We have selected these cell lines as HeLa is a cancer cell line that is extensively used for basic research purpose, while HEK293T cell line was selected as it is a normal transformed kidney cell line and used extensively across the world.

Human LIG4 gene contains two exons, but LIG4 coding sequence is present only in exon 2 (Fig. 1). For LIG4 gene inactivation, two single guide RNAs (sgRNAs) were designed, sgRNA1 targeted the nucleotide position 2424 (BRCT2 domain) and sgRNA2 targeted the nucleotide position 915 (NTD, nucleotidyltransferase domain) of exon 2 in human DNA LIG4 gene (Fig. 1A and B). Catalytic site of Ligase IV is present in the NTD domain at 819 nucleotide position. Both the sgRNAs were cloned into LentiCRISPRv2 backbone at *Bsm*BI restriction enzyme site resulting in generation of pNK1 (sgRNA1) and pNK2 (sgRNA2) construct (Fig. S1A and B). HeLa and HEK293T cells were transfected with pNK1 and pNK2 and selected for puromycin (0.5 μg/ml) resistant clones for three weeks (Fig. S1C). Only two and four wells containing HeLa and HEK293T cells, respectively showed presence of viable healthy cells. Genomic DNA was isolated from the puromycin resistant cells (HeLa, 2 and HEK293T, 4), region of interest was PCR amplified, cloned into TA vector, and sequenced (Fig. S1C). Results revealed deletion of 15 and 22 bp at PAM (protospacer adjacent motif) sequence of sgRNA2 at exon 2 resulting in a frameshift mutation in the LIG4 gene of one of the clones from HeLa cells, namely HeLa.Lig4.catDΔ.1.NK (indicated in the study as HeLa KO1 where KO stands for knock out) (Fig. 1C and F). In the second clone of HeLa cells, there were deletions of 10 nt downstream of PAM sequence of sgRNA1 and insertion of 1 bp near PAM sequence of sgRNA2, named as HeLa.Lig4.catDΔ.2.NK (indicated as HeLa KO2) (Fig. 1C and F). In case of HEK293T cells, there was insertion of thymine downstream to the PAM sequence of sgRNA1 in one clones, HEK293T. Lig4.catDΔ.1.NK (HEK293T KO1) (Fig. 1D and F). An insertion of 1 bp (thymine) at downstream to the PAM sequence of sgRNA2 and deletions of 9 bp near PAM sequence of sgRNA2 was observed in the other clone, HEK293T.Lig4.catDΔ.2.NK (HEK293T KO2) (Fig. 1E and F). Further, sequencing results of other two mutants of HEK293T showed presence of deletions of 15 bp and 9 bp and insertion of 1 bp at sgRNA2 and insertion of 1 bp near PAM sequence of sgRNA1, named as HEK293T.Lig4. catDΔ.3.NK (HEK293T KO3) (Fig. 1E and F), and insertion of 1 bp, deletions of 9 and 16 bp at the target site of sgRNA2 in other clone, HEK293T.Lig4.catDΔ.4.NK (HEK293T KO4) (Fig. 1E and F). Sequencing analysis also revealed that one of the alleles is wild type in some of the clones suggesting that clones obtained are not homozygous in nature. This may be due to the use of NHEJ for sealing of DSBs generated as part of CRISPR-Cas9 mediated genome editing.

Western blot analysis was performed to check the expression of Ligase IV protein in the LIG4 mutant cells. Our results showed significant reduction in the Ligase IV expression in HeLa KO1 and HeLa KO2 cells (Fig. 1G). Further in the case of HEK293T cells, highest reduction in Ligase IV expression was seen in HEK293T KO3 followed by HEK293T KO1 and minimum reduction in HEK293T KO2 cells (Fig. 1H). PCNA was used as loading control to normalize the Ligase IV expression. Thus, our results showed that all the clones generated from HeLa and HEK293T cells harboured different mutations and had different impact on Ligase IV expression. Hence, we were interested in characterizing all different mutants in terms of functional activity, cell viability, radiosensitivity, *etc.*

3.2. Mutation in LIG4 gene leads to reduced NHEJ activity both in vitro and within the cells

Since, Ligase IV is the key enzyme associated with NHEJ inside the cells, we investigated the impact of different mutations in LIG4 with respect to DNA end joining. In order to investigate the functional activity of Ligase IV protein in mutant cells, a cell-free repair assay system was utilized. Cell-free extracts (CFE) were prepared from LIG4 mutant and WT cell lines of HeLa and HEK293T. Equal concentration of CFE for joining assay was confirmed by loading on SDS PAGE (Fig. 2A and B). End joining assay was performed by incubating CFE from LIG4 mutant cells or WT cells with radiolabelled dsDNA substate with 5′ overhang (SCR19/20), joined products were purified and resolved on denaturing PAGE (Fig. 2C). Efficient end joined products of dimer (150 nt) and circular products (between 75 and 100 nt) were observed in case of extracts prepared from both HeLa and HEK293T WT cells (Fig. 2C, lanes 2, 5). In contrast, there was a significant reduction in the joining when DNA was incubated with extracts prepared from LIG4 mutant cells (Fig. 2C, lanes 3,4 and 6–9). Maximum inhibition of end joining was seen in case of HeLa cells KO1 and KO2 and HEK293T KO3, KO4 (Fig. 2C-E). Among the mutants, lowest inhibition was seen in the case of HEK293T KO1 and KO2. Thus, Ligase IV mutant cells exhibited varying levels of joining efficiency, which appears to be correlating with level of Ligase IV in the mutant cells.

Next, we were interested in examining the NHEJ efficiency within the LIG4 mutant cells using extrachromosomal assay [51,66,75]. To do this, NHEJ reporter construct, pimEJ5GFP containing disrupted GFP gene and I-*Sce*I sites was used as described before [75]. I-SceI induced DSBs within the episome can be repaired by NHEJ leading to the restoration of GFP expression (Fig. 2F). LIG4 mutant cells and WT HeLa and HEK293T were transiently transfected with pimEJ5GFP reporter and I-SceI overexpression constructs. Flow cytometry analysis revealed significantly reduced number of GFP positive cells in the LIG4 mutant cells compared to HeLa WT cell, which was comparable to the results obtained after end joining assay (Fig. 2G and Fig. S2). In the case of HEK293T KO3, KO4 and KO1 also showed a significant reduction in the number of GFP-positive recombinants compared to the WT cell (Fig. 2H and Fig. S2). Although a reduction was also seen in HEK293T KO2, it was less compared to other mutants. Thus, the functional assays conducted at *in vitro* and *ex vivo* level showed reduced levels of NHEJ in the LIG4 mutant cells in both cancer and normal cell lines.

3.3. Functional abrogation of NHEJ within cancer and normal cells lead to elevated MMEJ activity in LIG4 mutants

Previously, it has been reported that MMEJ rate goes high when NHEJ gene is mutated, as MMEJ occurs only in low frequency in normal cells [90]. Therefore, we hypothesized that loss of Ligase IV expression can result in increase in the MMEJ repair efficiency in the mutant cells. To test the hypothesis, we used an in-house developed PCR based MMEJ assay [12,30]. To do this, two double stranded oligomers containing a 10 nt microhomology regions (SS54/62 and SS65/66) were incubated with CFE from LIG4 mutant and WT cells. The joining using microhomology will result in 62 nt joined product which can be detected by radioactive PCR (Fig. 3A). A significant increase in the microhomology mediated end joining was observed in LIG4 mutant cells as compared to WT cells in the case of HeLa KO2, HEK293T KO3, KO4 and KO1, although the effect was minimal in the case of HEK293T KO2 (Fig. 3B-E). This result indicates that there is a significant increase in MMEJ efficiency when NHEJ is abrogated in human cancer and normal cells.

3.4. Disruption of LIG4 lead to enhanced HR activity

Based on the above results, we were interested in studying the level of HR in LIG4 mutant cells. To compare the recombination efficiency in WT HeLa, WT HEK293T and respective LIG4 mutant cells, we chose

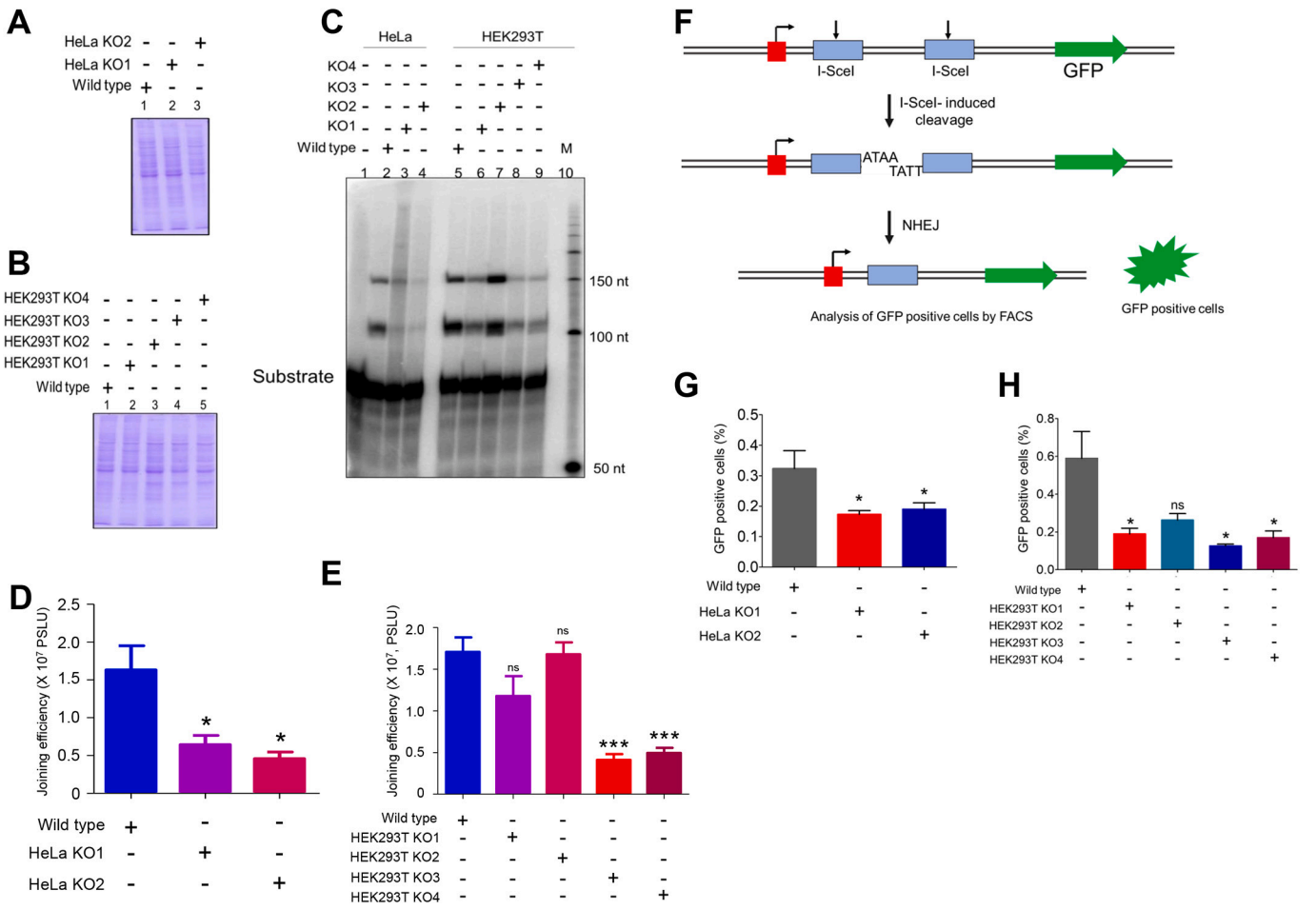

Fig. 2. Assessment of efficacy of NHEJ in LIG4 mutant cells both *in vitro* and within cells. A. SDS-PAGE profile showing equal concentration of cell-free extract prepared from HeLa WT (lane1) and HeLa KO1 (lane 2) and HeLa KO2 (lane 3) of LIG4 mutant cells. B. SDS-PAGE profile showing equal loading of cell-free extract prepared from HEK293T WT (lane1) and HEK293T KO1 (lane 2), HEK293T KO2 (lane 3), HEK293T KO3 (lane 4), and HEK293T KO4 (lane 5) of LIG4 mutant cells. C. Representative denaturing PAGE showing comparison of end joining when dsDNA (SCR19/20) was incubated with CFE (2 μg) prepared from LIG4 mutants of HeLa and HEK293T. 'M' represents 50 bp ladder. Lane 1 denotes radiolabelled ds DNA without CFE, lane 2 and 5 denotes joining efficiency with WT CFE D, E. Bar graphs showing quantitation of joining efficiency of HeLa WT and LIG4 mutants (D) and HEK293T WT and LIG4 mutants (E). Error bars indicate mean ± SEM plotted using three independent repeats, *** denotes $p < 0.0001$, * denotes $p < 0.05$ and ns depicts not significant. F. Schematic representation of intracellular NHEJ assay. PimEJ5GFP is the reporter construct containing disrupted GFP sequence flanked by I-*Sce*I sites. Upon transfection with I-SceI overexpression construct, break is induced in PimEJ5GFP and NHEJ mediated DSB repair of the construct can restore the GFP expression. G. Comparison of intracellular NHEJ activity in WT and LIG4 mutant HeLa cells. GFP positive cells were analyzed by flow cytometry and plotted as bar graph. H. Bar graph showing the intracellular NHEJ activity of HEK293T WT and LIG4 mutant cells. Percentage of GFP positive cells were obtained from three independent repeats and plotted as a bar graph showing mean ± SEM (ns: not significant, *$p < 0.05$).

HeLa KO1 and HEK293T KO3 cells. HR-mediated DSB repair was evaluated using plasmid-based assay system. pTO223 and pTO231 plasmids harbouring two independent mutations at neomycin gene were incubated with cell-free extracts prepared from respective cells in HR buffer and the purified DNA was used for transforming *E. coli* DH5α (Fig. 4A). Recombination catalysed by the extracts, will restore functional neomycin gene conferring resistance to kanamycin upon transformation into recombination deficient, *E. coli*. The recombinants were scored on ampicillin/kanamycin double resistant agar plates and recombination frequency was determined as the ratio of number of recombinants to the number of transformants. Results showed a recombination frequency of 4.2 ± 1.9 in the case of HeLa KO1, while it was 2.2 ± 0.7 in the case of HeLa WT (1.9-fold increase in recombination frequency). In the case of noncancerous cell line, HEK293T cells, LIG4 mutation resulted in 3.8-fold increase in the recombination frequency as compared to wild type cells (1.9 ± 0.1 in case of HEK293T WT and 7.3 ± 1.8 in case of HEK293T KO3) (Fig. 4B, C). Thus, our result showed a significant increase in homologous recombination frequency in LIG4 mutant cells as compared to WT cells in both HeLa as well as HEK293T cells (Fig. 4B, C). Restriction digestion analysis of kanamycin scored clones showed occurrence of HR mediated DSB repair *via* both gene conversion (~40%) and reciprocal exchange (~9%) (Fig. 4D). This result suggests that in absence of NHEJ, HR is elevated in both normal and cancer cells although the increase was more prominent in HEK293T LIG4 mutant cells as compared to HeLa cells (Fig. 4B, C). Overall, the results indicate that when NHEJ is abrogated, other DSB repair pathways are elevated and DSBs can be repaired by both MMEJ as well as HR pathways.

3.5. *LIG4 mutant cells show elevated levels of DSBs*

Ligase IV is involved in the final sealing of double-strand breaks during NHEJ and thus we were interested in testing whether LIG4 mutant cells harbour a greater number of breaks than WT cells. In order to investigate this, HeLa WT, HeLa KO1 and KO2 and HEK293T WT, HEK293T KO1, KO2, KO3 and KO4 were subjected to immunofluorescence (IF) studies using anti-γH2AX antibody. Compared to the WT cells, there was significant increase in the γH2AX foci in the LIG4 mutant HeLa cells (Fig. 5A-C). A comparable result was also observed in the case of

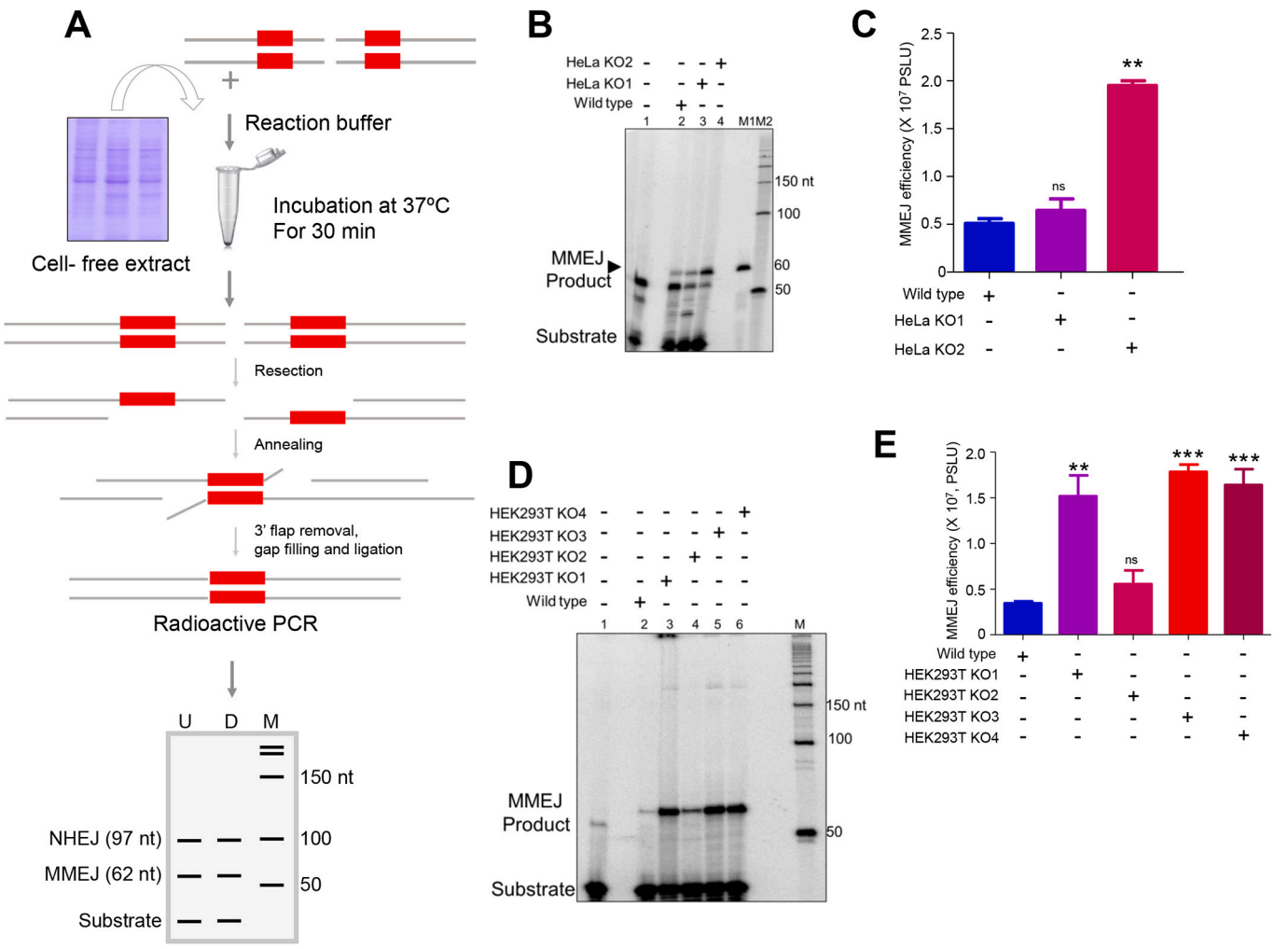

Fig. 3. Evaluation of efficacy of MMEJ in LIG4 mutant cells *in vitro*. A. Schematic representation of MMEJ assay. ds DNA substrate with 10 nt microhomology sequences were incubated with CFE for 30 min followed by PCR using radioactive primers and resolution of products on 10% denaturing PAGE. B. Representative denaturing PAGE profile showing comparison of MMEJ in WT HeLa and LIG4 mutant HeLa cells (HeLa KO1 and HeLa KO2). Lane 1 denotes ds DNA substrate without protein, lane 2 represents MMEJ product (62 nt) of WT CFE. 'M1' represents 60 bp radioactive DNA substrate and 'M2' represents 50 bp ladder. C. Bar graph showing quantitation of MMEJ products of HeLa WT and HeLa LIG4 mutant cells. D. Comparison of efficiency of MMEJ catalysed by CFE prepared from wild type and LIG4 mutant HEK293T cells. Lane 1 denotes ds DNA substrate without protein, lane 2 represents MMEJ product (62 nt) of HEK293T WT CFE. 'M' represents 50 bp ladder. E. Bar graph showing quantitation of MMEJ products of HEK293T WT and HEK293T LIG4 mutant cells. Error bars indicate mean ± SEM, *** denotes $p < 0.0001$, and ns depicts not significant.

HEK293T cells as well (Fig. 5A, D, E). WT cells also showed a smaller number of γH2AX foci, because of basal level of DNA damage generated by intracellular activities such as induction of ROS due to metabolism. However, as compared to WT cells, LIG4 mutant cells showed significant increase in basal level of γH2AX foci in all LIG4 mutants (Fig. 5A-E). Thus, our results suggest that due to functional abrogation of NHEJ, levels of unrepaired DSBs are higher in LIG4 mutant cells. Although, LIG4 depleted cells have been shown previously to lack end joining activity, accumulation of DSBs inside the cell was not reported before.

3.6. LIG4 mutants showed significant reduction in cell survival and sensitivity towards DNA damaging agents

Above results showed accumulation of DSBs in LIG4 mutant cells, therefore we wondered if there is any difference in cell survival/viability between WT and LIG4 mutant cells of cancer and normal cells. Towards this, equal number of WT and LIG4 mutant cells of HeLa and HEK293T cells were seeded on day 0 and cell viability was determined by trypan blue dye exclusion assay on each day over the course of five days. To our surprise, LIG4 mutant cells showed significant slower growth rate as compared to WT cells (Fig. 6A, B). The effect was more pronounced in the case of cancer cells compared to normal cells (Fig. 6A, B). Cell proliferation/survival was slower in all the clones of LIG4 starting from day 1 but the drastic effect was seen on fifth day especially in HeLa KO1 and 2 and HEK293T KO3 and 4 (Fig. 6A, B). However, the effect was minimal in the case of HEK293T KO1 and 2 (Fig. 6B). We also confirmed the cell survival by using alamar blue assay for 24, 48 and 72 h and results observed were comparable (Fig. 6C, D). This result was surprising since previously generated LIG4 null cell lines in pre-B lymphoid cell line did not show any significant difference in cell viability [33]. However, DT40 chicken B-lymphocyte Ligase IV$^{-/-}$ cells has been shown to proliferate at slightly slower rate compared to the WT cells [60]. Similarly, HCT116 LIG4 KO cells showed slower growth rate compared to the WT [91]. The difference in cell viability of LIG4 mutant in different cell types suggests that the dependency of cells on LIG4 can vary depending on the type of cells and their lineage. It was shown that embryonic lethality of Ligase IV deficient mice can be rescued by defective p53 [92]. Considering that both the cell lines used in the study do possess p53 mutation, the observed cell viability particularly at early time points such as 24 and 48 h could be explained.

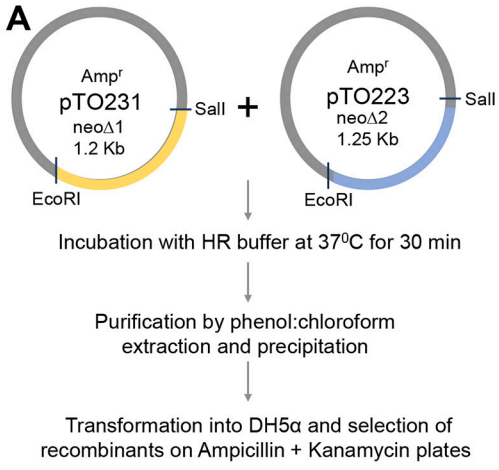

B

Protein extract	Ampicillin colonies ($X10^7$)	Kanamycin colonies	Recombination frequency ($X10^{-5}$)
No protein control	9.6	1	0.1 ± 0.1
HeLa WT	10.1	22	2.2 ± 0.7
HeLa KO1	8.8	38	4.2 ± 1.9
HEK293T WT	11.6	23	1.9 ± 0.1
HEK293T KO3	5.6	41	7.3 ± 1.8

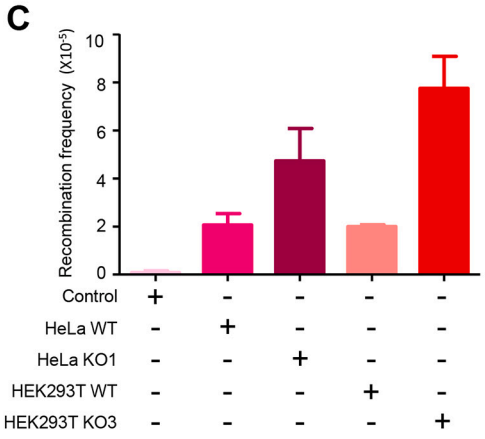

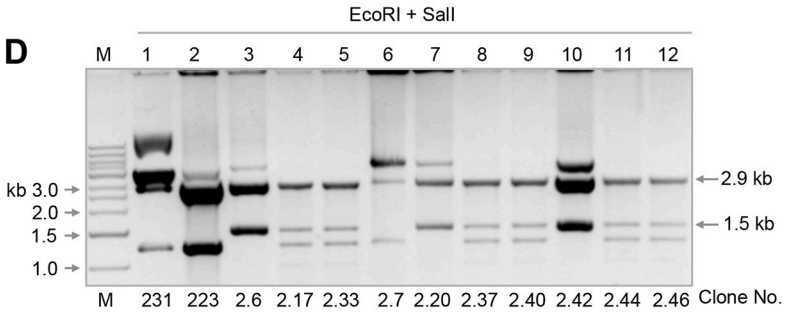

Fig. 4. Evaluation of efficiency of HR-mediated repair in LIG4 mutant cells. A. Schematic representation of HR assay. Two plasmid DNA substrates pTO231 and pTO223 harbouring independent neomycin mutations were incubated with cell-free extracts (1 μg) of HeLa and HEK293T WT and HeLa KO1 and HEK293T KO3 in HR buffer at 37 °C (for 30 min). The reaction was terminated, products were purified, and transformed into HR deficient *E. coli* cells followed by selection on ampicillin/kanamycin plates to evaluate recombinants. B. Table showing comparison of HR efficiency of HeLa WT with that of HeLa KO1, and HEK293T KO3 and its respective wildtype cells extract. Recombination frequency was calculated by dividing number of recombinants with number of transformants obtained after transformation. No protein control served as negative control, which accounts for background recombination catalysed in *E. coli*. C. Bar graph showing comparison of recombination frequency between WT and respective LIG4 mutant cells. Control represents no protein control which was used as the negative control. The graph was plotted using GraphPad Prism and the results depict mean ± SEM. D. Representative agarose gel image showing the *Eco*RI and *Sal*I digested recombinants (1.5 kb released fragment). 2.9 kb shows the vector backbone obtained after digestion. The plasmid DNA was isolated from clones obtained from HeLa WT, HeLa KO1, HEK293T WT and HEK293T KO3 after transformation of purified HR assay products and were subjected to EcoRI and SalI digestion followed by agarose gel electrophoresis. 231 and 232 represents digested plasmids pTO231 and pTO223, respectively. Clone No. indicates the name of the clone. "M" represents the molecular weight marker.

Further, the impact of DSB inducing agents on cell viability of LIG4 mutant cells was investigated. We chose two different DSBs inducing agents for this, ionizing radiation (IR) and etoposide. To check the sensitivity towards IR, 2.5×10^4 of WT and LIG4 mutant cells of both HeLa and HEK293T were seeded and exposed with increasing dose of IR (0.5, 1 and 2 Gy) and cell viability was assayed after 48 h using trypan blue exclusion assay. Our result showed dose dependent cell death in wild type as well as LIG4 mutant cells (Fig. 6E, F). Interestingly, LIG4 mutant cells showed significant increase in sensitivity towards IR compared to WT cells in dose dependent manner in both the cell lines. At highest dose of 2 Gy almost all the cells were dead in LIG4 mutant cells especially in HeLa KO1, KO2, and HEK293T KO3 cells (Fig. 6E, F). Similarly, LIG4 mutant cells were treated with etoposide (0.1, 0.25, 0.5 and 1 μM) and cell viability was assayed after 48 h. Results showed concentration dependent decrease in cell viability in both wild type and LIG4 mutant cells of HeLa as well as HEK293T (Fig. 6G, H). Consistent to the above results, HeLa KO1, KO2 and HEK293T KO3 showed the maximum cell death with increasing concentration of etoposide (Fig. 6G, H). Thus, our results reveal that LIG4 KO of HeLa cells are more sensitive to DNA damaging agents compared to the normal cells.

Next, we wanted to check If there is accumulation of DNA damage after treating with DNA damaging agents such as etoposide. Neutral comet assay, in which migration of DNA away from the nucleus in the form of a tail indicates the extent of DNA breaks was used to confirm accumulation of DSBs after treating with etoposide. We treated the cells with 4 μM of etoposide and incubated for 4 h at 37 °C and then cells were harvested and processed for neutral comet assay. Post treatment with etoposide, DNA damage was quantified by olive moment. Results showed significant increase in olive movement in case of LIG4 mutants as compared to the wild type cells in the case of both HeLa and HEK293T cells (Fig. S3A—C). This result is consistent with the above findings that abrogation of Ligase IV expression can result in significant increase in number of DSBs within the cells.

3.7. LIG4 mutant cells exhibits reduced DSB repair kinetics and ectopic overexpression of Ligase IV saves from the accumulation of DSBs

Since, LIG4 mutant cells showed accumulation of DSBs leading to

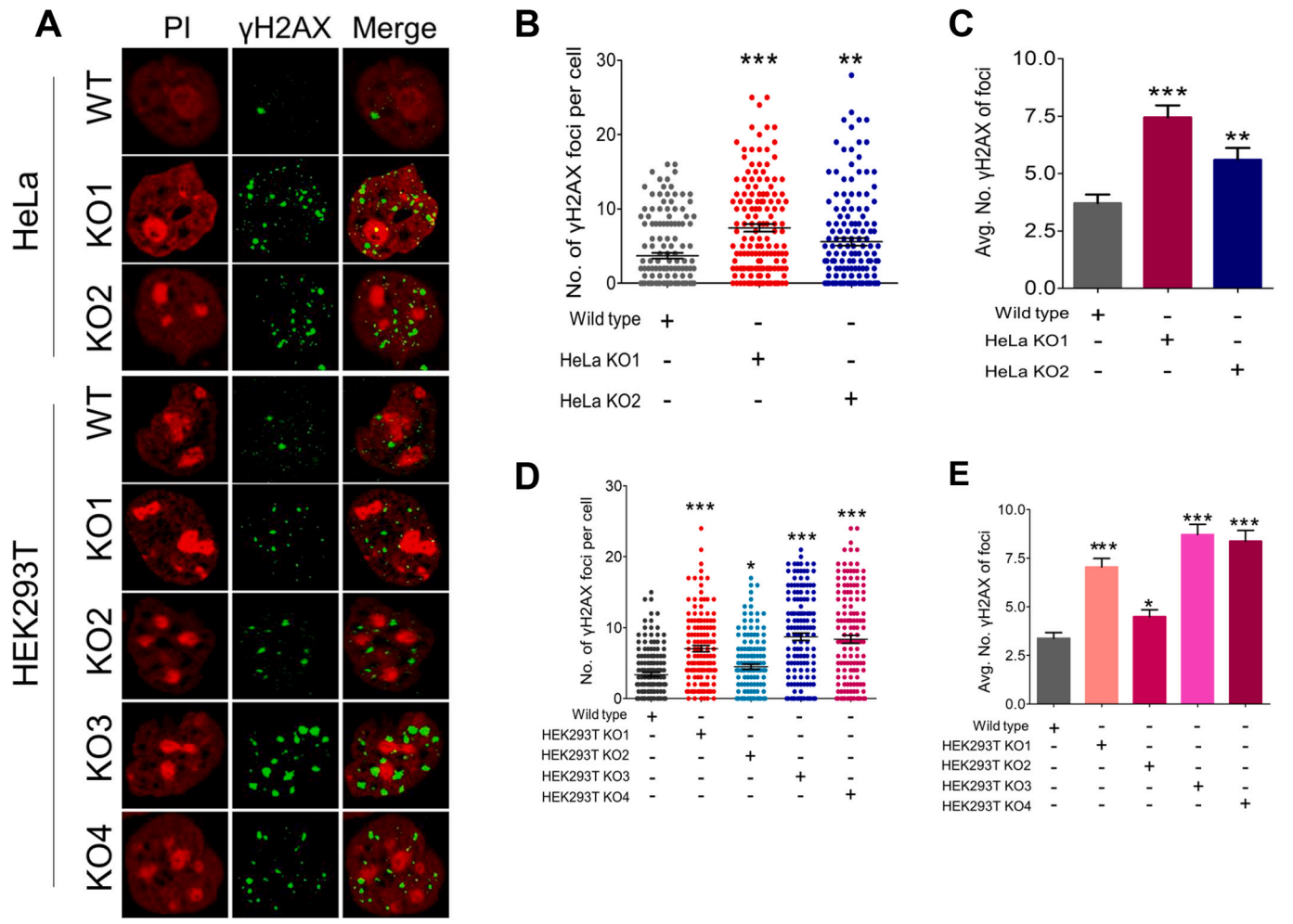

Fig. 5. Comparison of occurrence of endogenous DSBs in wild type and LIG4 mutant cells. A. Representative immunofluorescence images showing γH2AX foci as a marker for DSBs inside nucleus. WT and LIG4 mutant HeLa and HEK 293T cells were seeded on coverslip and accumulation of DSBs was scored by γH2AX foci (green) inside cells. Nucleus (red) was stained with propidium iodide. Merge image represents both the PI (red) and γH2AX (green) channels. B. Scatter plot showing the number of γH2AX foci per cell in HeLa WT and LIG4 mutant (HeLa KO1 and HeLa KO2) cells. Experiments were independently performed ($n = 3$) and ~ 100 cells were analyzed from each batch. Number of γH2AX foci were counted from individual cells and plotted using GraphPad Prism software. C. Bar graph showing quantification of average number of γH2AX foci per cell in HeLa WT and LIG4 mutant cells. D. Scatter plot for γH2AX foci in individual cells of HEK293T WT and LIG4 mutant HEK293T KO1, HEK293T KO2, HEK293T KO3, and HEK293T KO4 cells. Experiments were independently performed (n = 3) and a minimum of 100 cells were analyzed from each batch. E. Bar graph representing quantification of average number of γH2AX foci in HEK293T WT and LIG4 mutant cells. The results depict mean ± SEM; *** denotes $p < 0.0001$, ** denotes $p < 0.005$, and * denotes $p < 0.05$. (For interpretation of the references to colour in this figure legend, the reader is referred to the web version of this article.)

reduced cell survival, we were interested in investigating the effect of Ligase IV depletion on DSB repair kinetics. To do that, HeLa KO1 and HEK293T KO3 cells were chosen for the study along with respective WT cells as these mutants showed lowest Ligase IV expression and maximum defect in joining efficiency. WT and mutant cells were exposed to IR (2 Gy) and then performed immunofluorescence (IF) assay using anti-γ-H2AX at three different recovery time points (30 min, 6 h and 18 h). We observed significant γ-H2AX foci formation in both the WT and LIG4 mutant cells 30 min post IR in both WT and LIG4 mutant cells of HeLa and HEK293T cells (Fig. 7A-C). While a time dependent reduction in number of foci was observed in WT cells from HeLa and HEK293T, number of foci present in LIG4 mutant cells were significantly higher suggesting the radiosensitive nature of LIG4 mutant cells (Fig. 7A-C). Interestingly, 18 h post IR, most of the WT cells showed none or very few γ-H2AX foci indicating that almost all the DSBs have been repaired whereas the LIG4 mutants cell showed significantly higher number of γ-H2AX foci (Fig. 7A-C). These results suggest retarded DSB repair kinetics in LIG4 mutant cells.

Further, to establish that the defects seen in LIG4 mutant cells are specific, and indeed due to Ligase IV expression, we ectopically overexpressed Ligase IV in LIG4 mutant cells (HeLa KO1 and HEK293T KO3) and IF using anti-γ-H2AX was performed with and without exposure to IR. Results showed a significant increase in γ-H2AX foci in LIG4 mutant cells compared to WT following irradiation (Fig. 7D-F). Interestingly, upon overexpression of Ligase IV in LIG4 mutant cells, there was a significant reduction in the γ-H2AX foci in both HeLa KO1 and HEK293T KO3 cells. Ligase IV overexpression restored the number of γ-H2AX foci similar to the levels of WT cells (Fig. 7D-F). This result suggests that the observed elevated levels of DSBs are indeed due to mutation in LIG4 gene and is specific to Ligase IV.

3.8. *Reconstitution of end joining in LIG4 mutant cells by addition of purified Ligase IV/XRCC4 protein*

We have seen significantly reduced end joining in LIG4 mutant cells, when cell-free extracts were assayed for DNA end joining (Fig. 2A-E). To assess the reduction in joining efficiency observed was indeed due to lack of Ligase IV, we complemented the joining reaction with purified

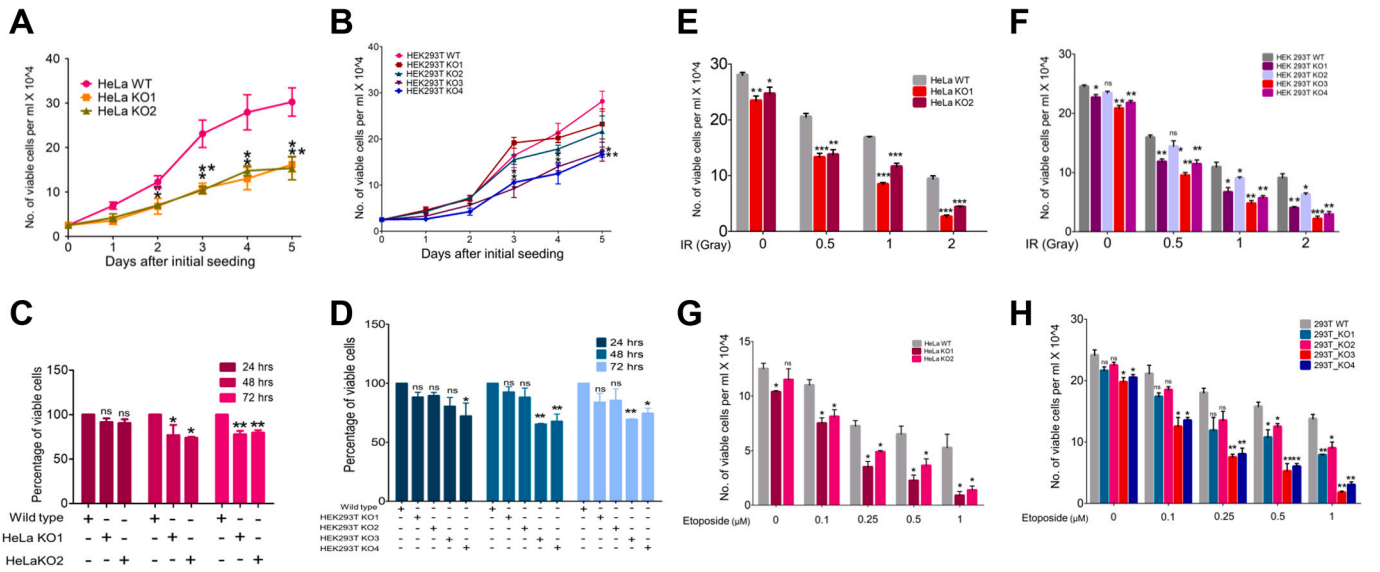

Fig. 6. Comparison of cell viability in LIG4 mutants of HeLa and HEK293T cells and cell viability following exposure to ionizing radiation and etoposide. A. Comparison of cell growth rate in HeLa WT and LIG4 mutant cells. Equal number of WT and LIG4 mutant cells (2.5×10^4) were seeded on day 0 and cell number was counted after every 24 h till day 5. Cell viability was monitored a minimum of 3 times, independently. B. Survival plot of HEK293T WT and HEK293T LIG4 mutant cells. Cells were seeded from both WT and mutant HEK293T cells and cell viability was monitored as described in panel B (n = 3). Survival plot was plotted using GraphPad Prism software and ** denotes $p < 0.005$, and * denotes $p < 0.05$. C. Bar graph showing the cell viability of HeLa WT and LIG4 mutant (HeLa KO1 and HeLa KO2) cells. Alamar blue assay was used to monitor the cell viability and absorbance was taken at 570 and 600 nm after 24, 48 and 72 h. D. Bar graph represents cell viability of HEK293T WT and LIG4 mutant (HEK293T KO1, HEK293T KO2, HEK293T KO3, and HEK293T KO4) cells. Alamar blue assay was used to check the cell viability as described in panel C. Absorbance was measured at 24, 48 and 72 h and plotted as bar graph showing mean ± SEM (ns: not significant, *p < 0.05, **p < 0.005). E, F. Bar graph depicting the comparison of cell viability of WT and LIG4 mutant HeLa (E) and HEK293T (F) cells after 48 h of exposure to increasing dose of irradiation (0.5, 1, and 2 Gy). G, H. Comparison of cell viability of WT and LIG4 mutant cells of HeLa (G) and HEK293T (H) after 24 h of exposure to increasing dose of etoposide (0.1, 0.25, 0.5 and 1 μM). In panels *E*-H, experiments were performed three times independently and plotted using GraphPad Prism (ns: not significant, *p < 0.05, **p < 0.005, *** denotes $p < 0.0001$). (For interpretation of the references to colour in this figure legend, the reader is referred to the web version of this article.)

Ligase IV/XRCC4. His-tagged human Ligase IV/XRCC4 was purified using Ni-NTA column, purity of the protein was checked on SDS-PAGE by CBB staining (Fig. S4A). Purified Ligase IV/XRCC4 was incubated with CFE of LIG4 mutant cell lines and dsDNA substrate along with other control reactions. Purified reaction product was resolved on 8% denaturing PAGE and radioactive signals were determined (Fig. S4B). Results showed restoration of end joining in LIG4 mutant extract of both HeLa as well as HEK293T cells following addition of purified Ligase IV/XRCC4 (Fig. 7G, H). Reconstituted end joining activity was comparable to that of WT cells in case of both the cell lines. These results showed that defects in DNA end joining of LIG4 mutant cells were indeed Ligase IV specific and not due to any off-target effect of CRISPR-Cas9 mediated gene editing.

3.9. Mutations in LIG4 gene results in synthesis of truncated Ligase IV protein

To check the effect of LIG4 mutation on Ligase IV protein structure, we chose modelling of Ligase IV proteins from HeLa KO1 and HEK293T KO3 mutants. Amino acid sequence was obtained from EXPASY translate tool based on the DNA sequencing data (Fig. 2C-F) and mutant Ligase IV protein structures were generated using SWISS-MODEL. Wild type full length Ligase IV protein was obtained from PDB (PDB ID: 3W50) and textured using 3D builder (Fig. 8A, B). HeLa KO1 contained deletions of 22 nucleotide in the exon 2 and 324 amino acid truncated Ligase IV sequence (Fig. 8C, D). Similarly, HEK293T KO3 contained deletions of 15 nucleotide in Ligase IV sequence and resulted in truncated 307 amino acid sequence (Fig. 8E, F). Further, we also obtained the protein structures of HeLa KO2 and HEK293T KO4 (Fig. S5A—F). The folded protein contained the catalytic site but resulted in deletions of oligonucleotide/oligosaccharide-fold (OBD) subdomains, BRCT1 and BRCT2 domain (Fig. 8). These results suggest that due to the absence of DNA binding domain, truncated Ligase IV would not be able to bind to the DNA and perform the function.

3.10. HeLa cells with LIG4 mutation exhibits enhanced cytotoxicity against FDA-approved drugs used for cervical cancer treatment

Results so far suggested that mutation in LIG4 gene can sensitize cells towards the DNA damaging agents. Based on that we were interested in studying the effect of different FDA approved drugs used against cervical cancer treatment, in cervical cancer cell line when LIG4 is mutated. It has also been shown that out of 54 cervical cancer patients, 5 cases indeed harboured mutation in Ligase IV gene [44]. Therefore, we sought to evaluate cytotoxic effect of different FDA approved drugs in LIG4 mutant HeLa cells. To understand the cytotoxic effect of various FDA approved drugs used in cervical cancer treatment, HeLa cells were treated with Cisplatin, Carboplatin, Bleomycin and Paclitaxel. Other drugs including Doxorubicin, 5-FU (5- Fluorouracil), Azacytidine *etc.* was also used for the study. Our results showed significant increase in cell death in a concentration dependent manner when different drugs were exposed in LIG4 mutant cells and in Hela WT cells (Fig. 9A and Fig. S6). As expected, HeLa cells showed decrease in viability upon exposure to FDA approved drugs (Fig. 9A). Drugs which are used against other cancer such as Azacytidine and 5-FU (Fig. 9A) showed low cell death. However, Doxorubicin showed similar effect as other cervical cancer drugs. In addition to that, small molecule inhibitor, Mirin which is inhibitor of MRE11 involved in HR also showed significant cell death in HeLa WT and LIG4 mutant cells (Fig. 9A).

Further, we were interested in analysing the effect of drugs in combination against cervical cancer cells when LIG4 is mutated. Significantly increased cell death was observed with the different

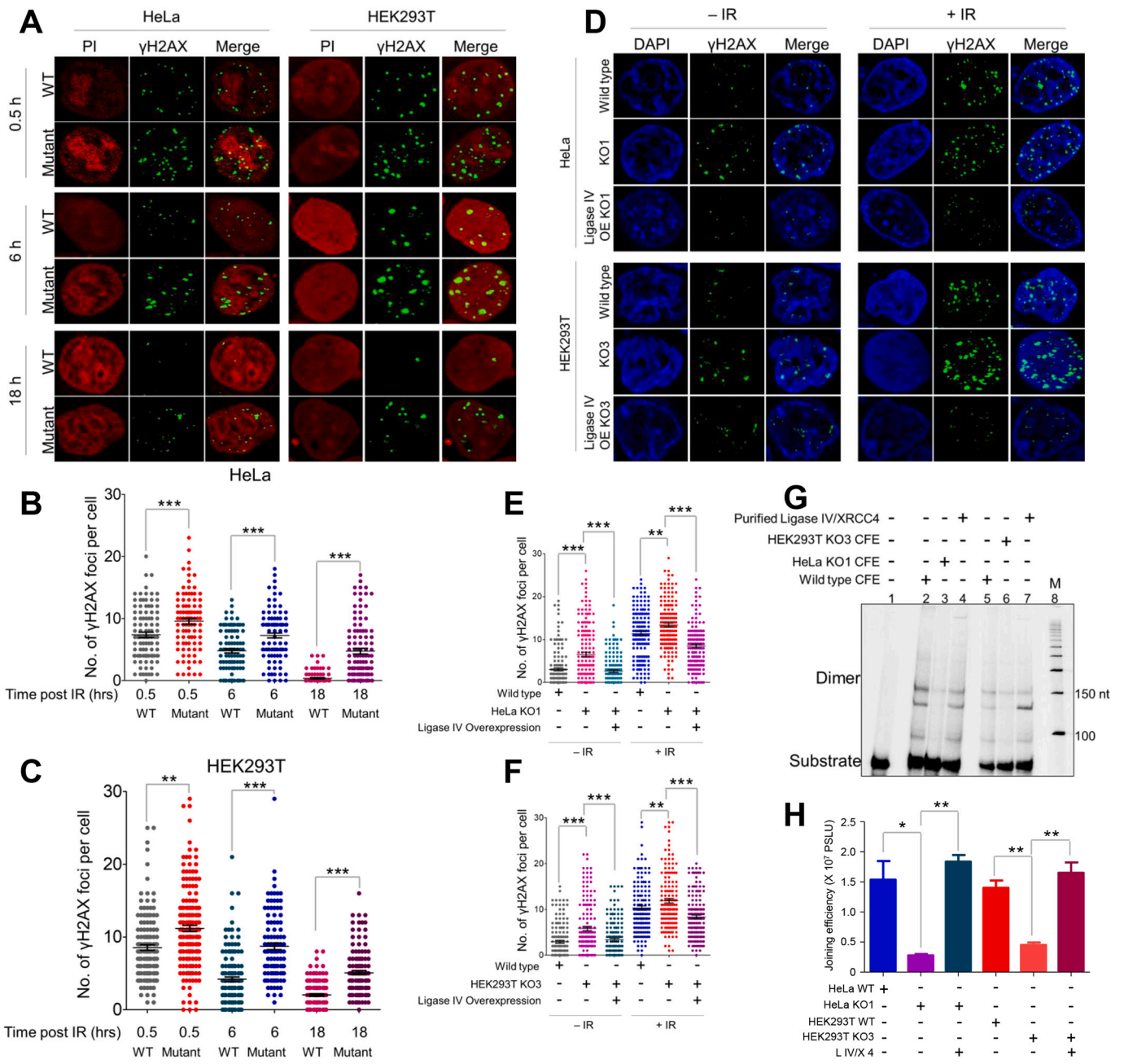

Fig. 7. Assessment of DSB repair kinetics following IR-induced breaks and functional analysis of Ligase IV specificity in LIG4 mutant. A. Representative IF images showing DSB repair kinetics of γH2AX foci in HeLa (left panel) and HEK293T (right panel) in WT and LIG4 mutant cells. WT and Ligase IV mutant cells were irradiated (2 Gy; recovery of 30 min, 6 h and 18 h) and stained with γH2AX in green (Alexa fluor 488) and nucleus in red (PI). Merged image showing colocalization of nucleus and γH2AX foci. Top panel are the representative images of 0.5 h, middle panel for 6 h and bottom panel for 18 h recovery after irradiation. B. Scatter plot showing quantification of number of γH2AX foci per cell in HeLa WT and LIG4 mutant (HeLa KO1) cells at three different time points of recovery (0.5, 6 and 18 h). C. Scatter plot representing the number of γH2AX foci per cell in HEK293T WT and LIG4 mutant (HEK293T KO3) cells after different time points of recovery (0.5, 6 and 18 h). In panels B, C, three independent batch of experiments were performed and >100 cells from each sample were counted and plotted using GraphPad Prism software depicting mean ± SEM (***denotes $p < 0.0001$, **denotes $p < 0.005$). D. Representative immunofluorescence images showing rescue of DSB accumulation (γH2AX foci; green, Alexa flour 488) after ectopic expression of Ligase IV in HeLa KO1 (top panel) and HEK293T KO3 (bottom panel) LIG4 mutant cells with and without exposure to IR (2 Gy). Nucleus was stained with DAPI (blue) and merge is the image from both the channels. 'OE' represents overexpression of Ligase IV protein in LIG4 mutant cells. E. Scatter plot represents the number of γH2AX foci in HeLa WT and HeLa KO1 with and without IR and after overexpression of Ligase IV in HeLa KO1. F. Scatter plot depicting γH2AX foci in HEK293T WT and HEK293T KO3 with and without irradiation and before and after overexpression of Ligase IV in HEK293T KO3 cells. Experiment was independently performed (n = 3) and >100 number of cells were counted from each set and plotted using GraphPad Prism software depicting mean ± SEM (*** denotes $p < 0.0001$, ** denotes $p < 0.005$). G. Denaturing PAGE profile showing restoration of NHEJ activity in CFEs prepared from LIG4 mutant HeLa KO1 (left panel) and HEK293T KO3 (right panel). Lane 1 denotes radiolabelled ds DNA without CFE, lanes 2 and 5 denotes joining efficiency with WT CFE of HeLa and HEK293T, respectively and lanes 3 and 6 denotes joining efficiency with HeLa KO1 and HEK293T KO3, respectively, lanes 4 and 7 are with addition of purified Ligase IV protein along with CFE of HeLa KO1 and HEK293T KO3, respectively. 'M' denotes 50 bp ladder. H. Bottom panel represents bar graph showing the quantitation of joining efficiency from three repeats of HeLa and HEK293T WTs and LIG4 mutants (with and without purified Ligase IV/XRCC4). Bar graph was plotted using GraphPad Prism depicting mean ± SEM (*$p < 0.05$ and **$p < 0.005$,). (For interpretation of the references to colour in this figure legend, the reader is referred to the web version of this article.)

A Amino acid sequence of full-length Ligase IV

```
MAASQTSQTVASHVPFADLCSTLERIQKSKGRAEKIRHFREFLDSWRKFHDALHKNHKDVTDSFYPAMRLILPQLERERMA
YGIKETMLAKLYIELLNLPRDGKDALKLLNYRTPTGTHGDAGDFAMIAYFVLKPRCLQKGSLTIQQVNDLLDSIASNNSAK
RKDLIKKSLLQLITQSSALEQKWLIRMIIKDLKLGVSQQTIFSVFHNDAAELHNVTTDLEKVCRQLHDPSVGLSDISITLF
SAFKPMLAAIADIEHIEKDMKHQSFYIETKLDGERMQMHKDGDVYKYFSRNGYNYTDQFGASPTEGSLTPFIHNAFKADIQ
ICILDGEMMAYNPNTQTFMQKGTKFDIKRMVEDSDLQTCYCVFDVLMVNNKKLGHETLRKRYEILSSIFTPIPGRIEIVQK
TQAHTKNEVIDALNEAIDKREEGIMVKQPLSIYKPDKRGEGWLKIKPEYVSGLMDELDILIVGGYWGKGSRGGMMSHFLCA
VAEKPPPGEKPSVFHTLSRVGSGCTMKELYDLGLKLAKYWKPFHRKAPPSSILCGTEKPEVYIEPCNSVIVQIKAAEIVPS
DMYKTGCTLRFPRIEKIRDDKEWHECMTLDDLEQLRGKASGKLASKHLYIGGDDEPQEKKRKAAPKMKKVIGIIEHLKAPN
LTNVNKISNIFEDVEFCVMSGTDSQPKPDLENRIAEFGGYIVQNPGPDTYCVIAGSENIRVKNIILSNKHDVVKPAWLLEC
FKTKSFVPWQPRFMIHMCPSTKEHFAREYDCYGDSYFIDTDLNQLKEVFSGIKNSNEQTPEEMASLIADLEYRYSWDCSPL
SMFRRHTVYLDSYAVINDLSTKNEGTRLAIKALELRFHGAKVVSCLAEGVSHVIIGEDHSRVADFKAFRRTFKRKFKILKE
SWVTDSIDKCELQEENQYLI
```

B

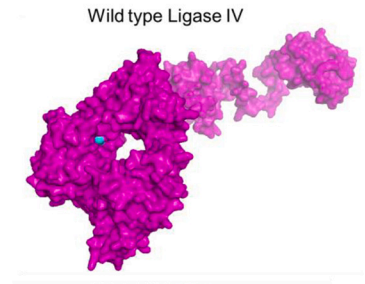

C Amino acid sequence of truncated Ligase IV in HeLa KO1

```
MAASQTSQTVASHVPFADLCSTLERIQKSKGRAEKIRHFREFLDSWRKFHDALHKNH
KDVTDSFYPAMRLILPQLERERMAYGIKETMLAKLYIELLNLPRDGKDALKLLNYRT
PTGTHGDAGDFAMIAYFVLKPRCLQKGSLTIQQVNDLLDSIASNNSAKRKDLIKKSL
LQLITQSSALEQKWLIRMIIKDLKLGVSQQTIFSVFHNDAAELHNVTTDLEKVCRQL
HDPSVGLSDISITLFSAFKPMLAAIADIEHIEKDMKHQSFYIETKLDGERMQMHKDG
DVYKYFSRNGYNYTDQFGASPTFIMHSKQIYKSVFLMVR
```

D

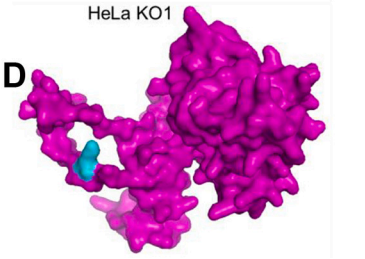

E Amino acid sequence of truncated Ligase IV in HEK293T KO3

```
MAASQTSQTVASHVPFADLCSTLERIQKSKGRAEKIRHFREFLDSWRKFHDALHKNHK
DVTDSFYPAMRLILPQLERERMAYGIKETMLAKLYIELLNLPRDGKDALKLLNYRTPT
GTHGDAGDFAMIAYFVLKPRCLQKGSLTIQQVNDLLDSIASNNSAKRKDLIKKSLLQL
ITQSSALEQKWLIRMIIKDLKLGVSQQTIFSVFHNDAAELHNVTTDLEKVCRQLHDPS
VGLSDISITLFSAFKPMLAAIADIEHIEKDMKHQSFYIETKLDGERMQMHKDGDVYKY
FSRNGYNYTDQFGASPT
```

F

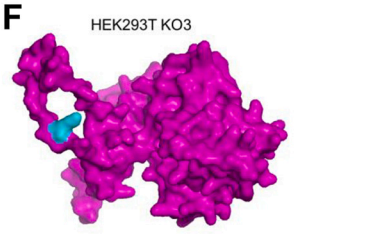

Fig. 8. Predicted structure of truncated Ligase IV protein LIG4 mutant cell lines. A, B. Amino acid sequence of full-length wild type Ligase IV protein (911 aa, A) and cartoon showing 3D crystal structure of full-length Ligase IV (B) obtained from PDB database and textured using 3D builder software. C, D. Amino acid sequence of truncated Ligase IV from HeLa KO1 (324 aa, C) and 3D crystal structure of truncated Ligase IV from HeLa KO1 (D). E, F. Amino acid sequence of truncated protein from HEK293T KO3 (307 aa, E) and 3D crystal structure of truncated Ligase IV from HEK293T KO3 (F). Cyan colour denotes the catalytic site of the Ligase IV protein. Structures for truncated LIG4 proteins in the figure were generated using SWISS-MODEL and textured in 3D builder. (For interpretation of the references to colour in this figure legend, the reader is referred to the web version of this article.)

combinations (Cisplatin and Carboplatin, Doxorubicin and Cisplatin, Paclitaxel and Cisplatin, Carboplatin and Paclitaxel, Doxorubicin and Paclitaxel and Doxorubicin and Carboplatin) in LIG4 mutant cells, compared to that of WT HeLa cells (Fig. 9B). Among the combinations, Cisplatin in combination with other drugs showed maximum effect leading to cancer cell death (Fig. 9B). These results indicate that cervical cancer with mutation in Ligase IV or any other DSBs repair pathway gene may be treated with combination of these FDA approved drugs. However, this requires further investigation.

Besides chemotherapy, radiotherapy is commonly used for the treatment of cervical cancer. We were interested in evaluating the effect of radiation with FDA approved drugs used in cervical cancer treatment in LIG4 mutant cells. For this, LIG4 mutant HeLa cells along with WT cells were exposed to IR (0.5 Gy) alone and in combination with different drugs Cisplatin (0.5 μM), Doxorubicin (0.01 nM), Paclitaxel (0.01 nM), Bleomycin (5 μM), and Carboplatin (0.5 μM) were used with 0.5 Gy IR. Results showed that LIG4 mutant cells were highly sensitive to radiation when used in combination with different drugs (Fig. 9C). For example, Cisplatin showed significant increase in cell death when used in combination with IR. We also calculated the fold change and found out that there was significant reduction in the combination of drugs with IR as compared to IR or drug alone. Among all the drugs Cisplatin and Bleomycin showed the maximum effect in LIG4 mutant cells in combination with IR (Fig. 9C). Although IR alone could induce cell death, combinatorial treatment with other drugs resulted in enhanced cell death in LIG4 mutant cells. These results suggest that radiation combined with drugs can induce significant cell death when DNA repair gene is mutated. All the above result suggests that cervical cancer patients with mutation in critical DNA repair gene can be treated with lower concentration of different FDA-approved drugs as well as with lower dose of radiation. Further, our data also reveal that radio and chemotherapy can be combined when there is mutation in DSB repair genes. However further studies are required to investigate the effect of different drugs in different mutants of DSBs repair genes of cervical cancer patients.

4. Discussion

In the present study we have developed different mutations in the LIG4 gene. Of that 2 were in cervical cancer cell line, HeLa, and other 4 in normal kidney epithelial cell line, HEK293T using CRISPR-Cas9 gene editing technology. Following cloning and sequencing of the mutations, the cellular impact of different LIG4 mutations were characterized at biochemical, cellular, and structural level. Finally, the therapeutic impact of the mutation was analyzed by treating the mutant cells with both DNA damaging agents and different FDA approved drugs.

Ligase IV is involved in the final ligation of broken ends of the DSBs during NHEJ and any change in the expression of Ligase IV will affect the joining activity. We found reduction in the end joining when cell-free extracts of Ligase IV mutant cells were used for the study (Fig. 2A-E). This result was similar with previous reports showing reduction in DSBs end joining when plasmid end joining was studied using CFEs from LIG4 mutant cells [58,93]. Results from our study revealed that level of Ligase IV expression varied between different

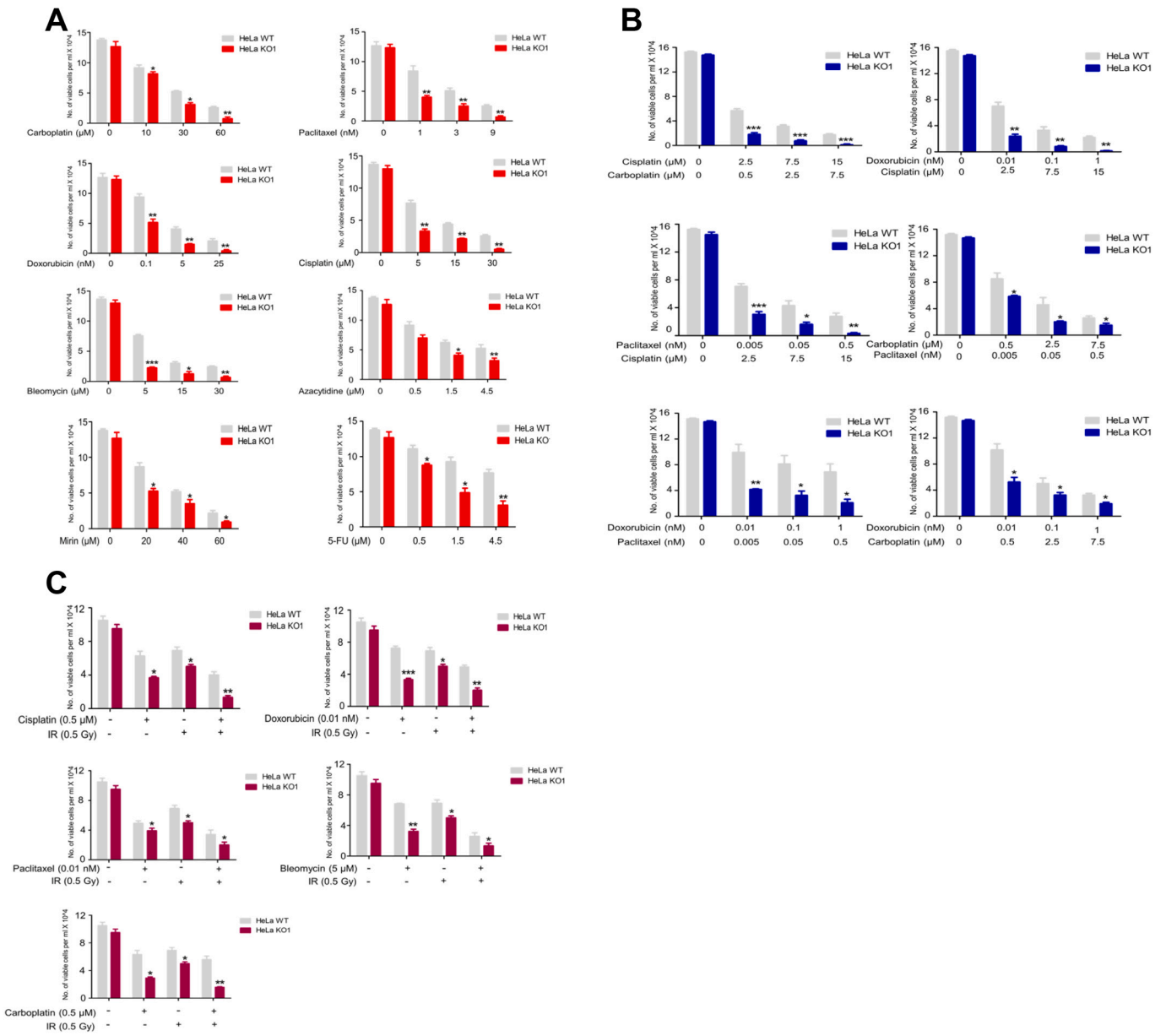

Fig. 9. Evaluation of cytotoxicity induced by different clinically relevant drugs and radiation either alone, or in combination in cervical cancer cells when LIG4 is mutated. *A. HeLa* WT and LIG4 mutant cells were treated with increasing concentration of clinically relevant FDA approved drugs, Carboplatin, Paclitaxel, Doxorubicin, Cisplatin, Bleomycin, Azacytidine and 5-FU and Mirin for 48 h. Cytotoxicity induced by the drug in the LIG4 mutant was evaluated and represented (n = 3). Bar graph showing cytotoxicity of Carboplatin (10, 30 and 60 μM), Paclitaxel (1, 3 and 9 nM), Doxorubicin (0.1, 5 and 25 nM), Cisplatin (5, 15 and 30 μM), Bleomycin (5, 15 and 30 μM), Azacytidine (0.5, 1.5 and 4.5 μM), mirin (20, 40 and 60 μM) and 5-FU (0.5, 1.5 and 4.5 μM). B. Cytotoxicity of HeLa WT and LIG4 mutant cells in combination using Cisplatin (2.5, 7.5 and 15 μM) with Carboplatin (0.5, 2.5 and 7.5 μM), and Doxorubicin (0.01, 0.1 and 1 nM) and Paclitaxel (0.005, 0.05 and 0.5 nM) with Cisplatin, and Carboplatin and, Doxorubicin with Paclitaxel, and Carboplatin. C. Representative bar graph for compounds and irradiation (IR) alone (0.5 Gy) and in combination with different compounds and IR. Cytotoxicity of HeLa WT and LIG4 mutant cells with Cisplatin alone (0.5 μM) and in combination with IR (0.5 Gy), Doxorubicin alone (0.01 nM) and in combination with IR (0.5 Gy), Paclitaxel alone (0.01 nM) and in combination with IR (0.5 Gy), Bleomycin alone (5 μM) and in combination with IR (0.5 Gy) and Carboplatin alone (0.5 μM) and in combination with IR (0.5 Gy). Experiments were performed at least 3 times and significance was calculated using GraphPad Prism. Bar graph denotes mean ± SEM (*p < 0.05, **p < 0.005, *** denotes p < 0.0001).

mutant cells and was inversely proportional to the efficacy of NHEJ mediated joining of DSBs. LIG4 mutant cells also showed reduced joining activity inside the cell using GFP reporter plasmid. While the LIG4 mutants of HeLa showed robust inhibition in NHEJ, two of the four HEK293T LIG4 mutants showed only moderate effect on NHEJ. Complementation studies by adding back purified Ligase IV showed restoration of end joining activity confirming that defect in joining activity was indeed due to defective Ligase IV (Fig. 7G).

Previous studies suggests that cells utilize MMEJ when there is a mutation in key factors of NHEJ pathway [12,90]. Our data revealed that when there is a mutation in LIG4 gene, cells utilized the backup pathway which was dependent on microhomology. Our results revealed significantly increased level of MMEJ on LIG4 KO cells (Fig. 3A-E). This can be explained as cells utilize LIG1/LIG3 for end joining and therefore enhanced MMEJ mediated joining activity, when Ligase IV function is abrogated. Interestingly, abrogation of LIG4 also resulted in enhanced HR activity (Fig. 4B-D). Furthermore, inactivation of Ligase IV activity inside the cells resulted in accumulation of DSBs in the LIG4 mutant cells which was due to reduced level of DSB repair and repair kinetics. Ectopic expression of Ligase IV in LIG4 mutant cells resulted in restoration of

DSBs repair activity and showed reduced γH2AX foci formation. Among the mutations generated in LIG4, HeLa KO1 and KO2 and HEK293 KO3 and 4 showed maximum impairment of NHEJ and thus accumulation of DNA breaks. The effect of various mutations in different clones was also reflected in the folding of Ligase IV protein, for example Hela KO1 and HEK293T KO3 containing 22 and 15 nucleotide deletions respectively, expressed truncated protein of Ligase IV (Fig. 1F and Fig. 8C-F).

Besides its role in NHEJ during end joining of DSBs, Ligase IV also plays a critical role during V(*D*)J recombination. Therefore, Ligase IV is one of the crucial enzymes associated with maintenance of genome and immune system. The critical function of Ligase IV can be explained by the fact that Ligase IV deficient mice are embryonic lethal [35,94]. In fact, there are no reports for Ligase IV null mutations in humans showing nonviable nature of Ligase IV null mutants. In contrast human cell lines with Ligase IV deficiency are mostly viable. Despite the viable nature of the cell line, the importance of LIG4 function was reflected in the compromised cell proliferation/survival of LIG4 mutant cells (Fig. 6A-D). Surprisingly, Grawunder et al., could not detect any difference in growth rate of Ligase IV deficient human pre-B cell line [33]. However reduced cell proliferation in LIG4 null HCT116 and DT40 chicken B-lymphocyte cell lines were reported previously [60,91], which was consistent with our results. The reduced cell proliferation in the presence of catalytically inactive Ligase IV could be due to induction of MMEJ joining activity, when Ligase IV function is impaired (Fig. 3A-E) which could result in increased deletions and other chromosomal abnormalities leading to genomic instability. The slower growth rate can also be explained by accumulation of DSBs (Fig. 5A-D) which can further activate cell cycle checkpoints or even apoptosis and cell death [95,96].

In a recent study, Goff *et al.*, has generated catalytic inactive LIG4 (K273A) HEK293T cells and observed that catalytic inactive LIG4 stimulates the activity of Ligase III protein inside the cells. This stimulation of Ligase III resulted in increased joining through Alt-NHEJ [97]. Consistent with their finding, we found an increase in MMEJ activity in our studies. However, the observed increase in MMEJ in our study was due to stimulation of Ligase III activity or not needs further investigation. Unlike the reported catalytic inactive LIG4 (K273A) by Goff *et al.*, LIG4 mutants HEK293T cells reported by us harboured the active catalytic site, K273 (Fig. 8), although the mutation resulted in truncation of Ligase IV protein as there was a change in reading frame.

CRISPR-Cas9 gene editing technology introduces the required alterations in the genome by introducing DSBs at which desired gene modifications is carried out by NHEJ. Previous studies have shown that knock-in efficiency of green fluorescence protein (GFP) in the brain neurons was enhanced by 3.6-fold upon small hairpin RNA (shRNA) mediated knockdown of Ligase IV [98]. Similarly, SCR7, a small molecule inhibitor of Ligase IV showed increased efficiency of HR from 1.4 to 19-fold in cell lines [99]. Recently, CRISPR-Cas9 mediated KO of Ligase IV in CHO cell line showed 9.2-fold increase in SSI (site-specific integration) efficiency [100]. Therefore, our LIG4 mutants can be utilized for site specific insertion or deletions of any other gene in HEK293T and HeLa cells [101,102].

Ligase IV is involved in the formation of phosphodiester bond during NHEJ. Failure in this process results in accumulation of unrepaired DSBs imposes serious threats to the survivability at an organism level. Accumulation of DSBs can lead to genomic instability, disorders (immunological, developmental and neurological), chromosomal deletions and rearrangements, cancer and cell death [9,103]. Defects in DNA repair genes have been shown to be associated with cancer pathogenesis. Mutational landscape and gene expression alterations analysis of several cancer types have revealed the association between genomic instability and dysregulation of DNA repair genes [41,104]. In the same line we wanted to check the therapeutic implications of LIG4 mutation. Since we observed reduced cell proliferation, we tested the impact of different FDA approved drugs used in the cervical cancer treatment on LIG4 mutant cells. Our results showed significant increase in cell death in LIG4 mutant cells compared to WT cells when different FDA approved drugs were used alone and in combination of drugs as well as with the combination of IR (Fig. 9). Based on our data, mutation in LIG4 can compromise the DNA repair and result in sensitizing these cells with other clinically relevant drugs. Interestingly, our results also showed that LIG4 mutant cells were more sensitive to lower concentration of many FDA approved drugs when used in combination. Therefore, results from above study could be exploited further to lower the dosage of cancer drugs and could minimize the side effects.

Radio and chemotherapy are widely used during cancer therapy. Targeted inhibition of repair pathways will act as novel strategy to induce accumulation of DSBs and hence cell death [105,106]. Targeted therapy in combination with radio and chemotherapy especially in relapsed or resistant cancers can enhance the sensitivity [107,108]. Our data implicates that mutation in a DNA repair pathway gene can be used for sensitizing the cells to combination of radiation and FDA-approved chemotherapeutic agents such as Carboplatin, Cisplatin, Paclitaxel, Doxorubicin, and Bleomycin. The significant increase in sensitivity of LIG4 mutants with these FDA approved drugs opens a new opportunity for improved therapy in the background of mutation in DNA repair genes. Considering that the LIG4 mutation is less frequent in cervical cancer patients and the mutations that we studied are not exactly the same as those reported in cervical cancer patients, further studies are required to understand the clinical relevance of present findings. However, based on the study, one may able to take advantage of mutations in any DNA repair genes within cancer cells in the context of clinically relevant drugs and help in potential enhancement of the therapeutics approach.

CRediT authorship contribution statement

Nitu Kumari: Conceptualization, Methodology, Investigation, Writing – original draft, Writing – review & editing. **Himanshu Antil:** Investigation. **Susmita Kumari:** Investigation. **Sathees C. Raghavan:** Conceptualization, Methodology, Writing – original draft, Writing – review & editing, Funding acquisition, Resources, Supervision.

Declaration of Competing Interest

Authors disclose that there is no conflict of interest.

Data availability

Data will be made available on request.

Acknowledgements

We thank Urbi Roy, Ujjayinee Ray and other members of SCR laboratory for critical reading and comments on the manuscript. We thank Confocal, and the FACS facility for their help. This work was supported by grants DAE (21/01/2016-BRNS/35074), DBT-COE (BT/PR/3458/COE/34/33/2015), IISc-DBT partnership program [BT/PR27952-INF/22/212/2018] to SCR. NK and SK are supported by Senior Research fellowships (SRF) from IISc.

Appendix A. Supplementary data

Supplementary data to this article can be found online at https://doi.org/10.1016/j.ygeno.2023.110731.

References

[1] J.H. Hoeijmakers, DNA damage, aging, and cancer, N. Engl. J. Med. 361 (2009) 1475–1485.
[2] S.M. Javadekar, S.C. Raghavan, Snaps and mends: DNA breaks and chromosomal translocations, FEBS J. 282 (2015) 2627–2645.

[3] M. Nambiar, S.C. Raghavan, Chromosomal translocations among the healthy human population: implications in oncogenesis, Cell. Mol. Life Sci. 70 (2013) 1381–1392.
[4] U. Ray, S.C. Raghavan, Nonhomologous DNA end joining in mammalian cells, in: R.A. Bradshaw, G.W. Hart, P.D. Stahl (Eds.), Encyclopedia of Cell Biology (Second Edition), Academic Press, Oxford, 2023, pp. 552–566.
[5] A. Ciccia, S.J. Elledge, The DNA damage response: making it safe to play with knives, Mol. Cell 40 (2010) 179–204.
[6] S.P. Jackson, J. Bartek, The DNA-damage response in human biology and disease, Nature 461 (2009) 1071–1078.
[7] D. Ghosh, S.C. Raghavan, Nonhomologous end joining: new accessory factors fine tune the machinery, Trends Genet. 37 (2021) 582–599.
[8] M.R. Lieber, The mechanism of double-strand DNA break repair by the nonhomologous DNA end-joining pathway, Annu. Rev. Biochem. 79 (2010) 181–211.
[9] U. Ray, S.C. Raghavan, Modulation of DNA double-strand break repair as a strategy to improve precise genome editing, Oncogene 39 (2020) 6393–6405.
[10] D.O. Warmerdam, R. Kanaar, Dealing with DNA damage: relationships between checkpoint and repair pathways, Mutat. Res. 704 (2010) 2–11.
[11] M. Srivastava, Sathees C. Raghavan, DNA double-strand break repair inhibitors as cancer therapeutics, Chem. Biol. 22 (2015) 17–29.
[12] S. Sharma, S.M. Javadekar, M. Pandey, M. Srivastava, R. Kumari, S.C. Raghavan, Homology and enzymatic requirements of microhomology-dependent alternative end joining, Cell Death Dis. 6 (2015), e1697.
[13] C.T. Yan, C. Boboila, E.K. Souza, S. Franco, T.R. Hickernell, M. Murphy, S. Gumaste, M. Geyer, A.A. Zarrin, J.P. Manis, K. Rajewsky, F.W. Alt, IgH class switching and translocations use a robust non-classical end-joining pathway, Nature 449 (2007) 478–482.
[14] R.B. West, M. Yaneva, M.R. Lieber, Productive and nonproductive complexes of Ku and DNA-dependent protein kinase at DNA termini, Mol. Cell. Biol. 18 (1998) 5908–5920.
[15] M. Yaneva, T. Kowalewski, M.R. Lieber, Interaction of DNA-dependent protein kinase with DNA and with Ku: biochemical and atomic-force microscopy studies, EMBO J. 16 (1997) 5098–5112.
[16] A.A. Goodarzi, Y. Yu, E. Riballo, P. Douglas, S.A. Walker, R. Ye, C. Härer, C. Marchetti, N. Morrice, P.A. Jeggo, S.P. Lees-Miller, DNA-PK autophosphorylation facilitates Artemis endonuclease activity, EMBO J. 25 (2006) 3880–3889.
[17] D. Niewolik, U. Pannicke, H. Lu, Y. Ma, L.C. Wang, P. Kulesza, E. Zandi, M. R. Lieber, K. Schwarz, DNA-PKcs dependence of Artemis endonucleolytic activity, differences between hairpins and 5′ or 3′ overhangs, J. Biol. Chem. 281 (2006) 33900–33909.
[18] D. Ghosh, S.C. Raghavan, 20 years of DNA polymerase μ, the polymerase that still surprises, FEBS J. 288 (2021) 7230–7242.
[19] D.A. Ramsden, Polymerases in nonhomologous end joining: building a bridge over broken chromosomes, Antioxid. Redox Signal. 14 (2011) 2509–2519.
[20] U. Grawunder, M. Wilm, X. Wu, P. Kulesza, T.E. Wilson, M. Mann, M.R. Lieber, Activity of DNA ligase IV stimulated by complex formation with XRCC4 protein in mammalian cells, Nature 388 (1997) 492–495.
[21] Y. Ma, H. Lu, B. Tippin, M.F. Goodman, N. Shimazaki, O. Koiwai, C.L. Hsieh, K. Schwarz, M.R. Lieber, A biochemically defined system for mammalian nonhomologous DNA end joining, Mol. Cell 16 (2004) 701–713.
[22] S.K. Tadi, C. Tellier-Lebègue, C. Nemoz, P. Drevet, S. Audebert, S. Roy, K. Meek, J.B. Charbonnier, M. Modesti, PAXX is an accessory c-NHEJ factor that associates with Ku70 and has overlapping functions with XLF, Cell Rep. 17 (2016) 541–555.
[23] D. Ghosh, S. Kumari, S.C. Raghavan, Depletion of RNASEH2 activity leads to accumulation of DNA double-strand breaks and reduced cellular survivability in T cell leukemia, J. Mol. Biol. 434 (2022), 167617.
[24] J.M. Pryor, M.P. Conlin, J. Carvajal-Garcia, M.E. Luedeman, A.J. Luthman, G. W. Small, D.A. Ramsden, Ribonucleotide incorporation enables repair of chromosome breaks by nonhomologous end joining, Science 361 (2018) 1126–1129.
[25] M.R. Lieber, K. Yu, S.C. Raghavan, Roles of nonhomologous DNA end joining, V (D)J recombination, and class switch recombination in chromosomal translocations, DNA Repair (Amst) 5 (2006) 1234–1245.
[26] E.A. Motea, A.J. Berdis, Terminal deoxynucleotidyl transferase: the story of a misguided DNA polymerase, Biochim. Biophys. Acta 2010 (1804) 1151–1166.
[27] A.E. Tomkinson, D.S. Levin, Mammalian DNA ligases, Bioessays 19 (1997) 893–901.
[28] C. Prigent, M.S. Satoh, G. Daly, D.E. Barnes, T. Lindahl, Aberrant DNA repair and DNA replication due to an inherited enzymatic defect in human DNA ligase I, Mol. Cell. Biol. 14 (1994) 310–317.
[29] I.N. Shokolenko, R.Z. Fayzulin, S. Katyal, P.J. McKinnon, G.L. Wilson, M. F. Alexeyev, Mitochondrial DNA ligase is dispensable for the viability of cultured cells but essential for mtDNA maintenance, J. Biol. Chem. 288 (2013) 26594–26605.
[30] S.K. Tadi, R. Sebastian, S. Dahal, R.K. Babu, B. Choudhary, S.C. Raghavan, Microhomology-mediated end joining is the principal mediator of double-strand break repair during mitochondrial DNA lesions, Mol. Biol. Cell 27 (2016) 223–235.
[31] A.E. Tomkinson, L. Chen, Z. Dong, J.B. Leppard, D.S. Levin, Z.B. Mackey, T. A. Motycka, Completion of base excision repair by mammalian DNA ligases, Prog. Nucleic Acid Res. Mol. Biol. 68 (2001) 151–164.
[32] K. Paul, M. Wang, E. Mladenov, A. Bencsik-Theilen, T. Bednar, W. Wu, H. Arakawa, G. Iliakis, DNA ligases I and III cooperate in alternative non-homologous end-joining in vertebrates, PLoS One 8 (2013), e59505.
[33] U. Grawunder, D. Zimmer, P. Kulesza, M.R. Lieber, Requirement for an interaction of XRCC4 with DNA ligase IV for wild-type V(D)J recombination and DNA double-strand break Repairin vivo *, J. Biol. Chem. 273 (1998) 24708–24714.
[34] D. Bentley, J. Selfridge, J.K. Millar, K. Samuel, N. Hole, J.D. Ansell, D.W. Melton, DNA ligase I is required for fetal liver erythropoiesis but is not essential for mammalian cell viability, Nat. Genet. 13 (1996) 489–491.
[35] K.M. Frank, J.M. Sekiguchi, K.J. Seidl, W. Swat, G.A. Rathbun, H.L. Cheng, L. Davidson, L. Kangaloo, F.W. Alt, Late embryonic lethality and impaired V(D)J recombination in mice lacking DNA ligase IV, Nature 396 (1998) 173–177.
[36] N. Puebla-Osorio, D.B. Lacey, F.W. Alt, C. Zhu, Early embryonic lethality due to targeted inactivation of DNA ligase III, Mol. Cell. Biol. 26 (2006) 3935–3941.
[37] Y.F. Wei, P. Robins, K. Carter, K. Caldecott, D.J. Pappin, G.L. Yu, R.P. Wang, B. K. Shell, R.A. Nash, P. Schär, et al., Molecular cloning and expression of human cDNAs encoding a novel DNA ligase IV and DNA ligase III, an enzyme active in DNA repair and recombination, Mol. Cell. Biol. 15 (1995) 3206–3216.
[38] J.M. Pascal, DNA and RNA ligases: structural variations and shared mechanisms, Curr. Opin. Struct. Biol. 18 (2008) 96–105.
[39] C. Bernstein, A.R. Prasad, V. Nfonsam, H. Bernstein, DNA Damage, DNA Repair and Cancer, InTech Rijeka, Croatia, 2013.
[40] P. Bouwman, J. Jonkers, The effects of deregulated DNA damage signalling on cancer chemotherapy response and resistance, Nat. Rev. Cancer 12 (2012) 587–598.
[41] Y.K. Chae, J.F. Anker, B.A. Carneiro, S. Chandra, J. Kaplan, A. Kalyan, C.A. Santa-Maria, L.C. Platanias, F.J. Giles, Genomic landscape of DNA repair genes in cancer, Oncotarget 7 (2016) 23312–23321.
[42] U. Ray, S.C. Raghavan, Understanding the DNA double-strand break repair and its therapeutic implications, DNA Repair (Amst) 106 (2021), 103177.
[43] B. Kuschel, A. Auranen, S. McBride, K.L. Novik, A. Antoniou, J.M. Lipscombe, N. E. Day, D.F. Easton, B.A. Ponder, P.D. Pharoah, A. Dunning, Variants in DNA double-strand break repair genes and breast cancer susceptibility, Hum. Mol. Genet. 11 (2002) 1399–1407.
[44] L. Zammataro, S. Lopez, S. Bellone, F. Pettinella, E. Bonazzoli, E. Perrone, S. Zhao, G. Menderes, G. Altwerger, C. Han, B. Zeybek, A. Bianchi, A. Manzano, P. Manara, E. Cocco, N. Buza, P. Hui, S. Wong, A. Ravaggi, E. Bignotti, C. Romani, P. Todeschini, L. Zanotti, F. Odicino, S. Pecorelli, C. Donzelli, L. Ardighieri, R. Angioli, F. Raspagliesi, G. Scambia, J. Choi, W. Dong, K. Bilguvar, L. B. Alexandrov, D.A. Silasi, G.S. Huang, E. Ratner, M. Azodi, P.E. Schwartz, V. Pirazzoli, A.L. Stiegler, T.J. Boggon, R.P. Lifton, J. Schlessinger, A.D. Santin, Whole-exome sequencing of cervical carcinomas identifies activating ERBB2 and PIK3CA mutations as targets for combination therapy, Proc. Natl. Acad. Sci. U. S. A. 116 (2019) 22730–22736.
[45] T. Altmann, A.R. Gennery, DNA ligase IV syndrome; a review, Orphanet J. Rare Dis. 11 (2016) 137.
[46] A. Enders, P. Fisch, K. Schwarz, U. Duffner, U. Pannicke, E. Nikolopoulos, A. Peters, M. Orlowska-Volk, D. Schindler, W. Friedrich, B. Selle, C. Niemeyer, S. Ehl, A severe form of human combined immunodeficiency due to mutations in DNA ligase IV, J. Immunol. 176 (2006) 5060–5068.
[47] M. O'Driscoll, K.M. Cerosaletti, P.M. Girard, Y. Dai, M. Stumm, B. Kysela, B. Hirsch, A. Gennery, S.E. Palmer, J. Seidel, R.A. Gatti, R. Varon, M.A. Oettinger, H. Neitzel, P.A. Jeggo, P. Concannon, DNA ligase IV mutations identified in patients exhibiting developmental delay and immunodeficiency, Mol. Cell 8 (2001) 1175–1185.
[48] A.M. Kaminski, P.P. Tumbale, M.J. Schellenberg, R.S. Williams, J.G. Williams, T. A. Kunkel, L.C. Pedersen, K. Bebenek, Structures of DNA-bound human ligase IV catalytic core reveal insights into substrate binding and catalysis, Nat. Commun. 9 (2018) 2642.
[49] X. Chen, S. Zhong, X. Zhu, B. Dziegielewska, T. Ellenberger, G.M. Wilson, A. D. MacKerell Jr., A.E. Tomkinson, Rational design of human DNA ligase inhibitors that target cellular DNA replication and repair, Cancer Res. 68 (2008) 3169–3177.
[50] U. Ray, V.K. Gopinatha, S. Sharma, L. Goyary, B. Choudhary, K. Mantelingu, K. S. Rangappa, S.C. Raghavan, Identification and characterization of mercaptopyrimidine-based small molecules as inhibitors of nonhomologous DNA end joining, FEBS J. 290 (2023) 796–820.
[51] M. Srivastava, M. Nambiar, S. Sharma, S.S. Karki, G. Goldsmith, M. Hegde, S. Kumar, M. Pandey, R.K. Singh, P. Ray, R. Natarajan, M. Kelkar, A. De, B. Choudhary, S.C. Raghavan, An inhibitor of nonhomologous end-joining abrogates double-strand break repair and impedes cancer progression, Cell 151 (2012) 1474–1487.
[52] S.V. Vartak, H.A. Swarup, V. Gopalakrishnan, V.K. Gopinatha, V. Ropars, M. Nambiar, F. John, S.K.S. Kothanahally, R. Kumari, N. Kumari, U. Ray, G. Radha, D. Dinesh, M. Pandey, H. Ananda, S.S. Karki, M. Srivastava, J. B. Charbonnier, B. Choudhary, K. Mantelingu, S.C. Raghavan, Autocyclized and oxidized forms of SCR7 induce cancer cell death by inhibiting nonhomologous DNA end joining in a ligase IV dependent manner, FEBS J. 285 (2018) 3959–3976.
[53] V. Gopalakrishnan, S. Sharma, U. Ray, M. Manjunath, D. Lakshmanan, S. V. Vartak, V.K. Gopinatha, M. Srivastava, M. Kempegowda, B. Choudhary, S. C. Raghavan, SCR7, an inhibitor of NHEJ can sensitize tumor cells to ionization radiation, Mol. Carcinog. 60 (2021) 627–643.
[54] U. Ray, S.K. Raul, V.K. Gopinatha, D. Ghosh, K.S. Rangappa, K. Mantelingu, S. C. Raghavan, Identification and characterization of novel SCR7-based small-molecule inhibitor of DNA end-joining, SCR130 and its relevance in cancer therapeutics, Mol. Carcinog. 59 (2020) 618–628.

[55] C. Badie, M. Goodhardt, A. Waugh, N. Doyen, N. Foray, P. Calsou, B. Singleton, D. Gell, B. Salles, P. Jeggo, C.F. Arlett, E.P. Malaise, A DNA double-strand break defective fibroblast cell line (180BR) derived from a radiosensitive patient represents a new mutant phenotype, Cancer Res. 57 (1997) 4600–4607.
[56] C. Badie, G. Iliakis, N. Foray, G. Alsbeih, G.E. Pantellias, R. Okayasu, N. Cheong, N.S. Russell, A.C. Begg, C.F. Arlett, et al., Defective repair of DNA double-strand breaks and chromosome damage in fibroblasts from a radiosensitive leukemia patient, Cancer Res. 55 (1995) 1232–1234.
[57] E. Riballo, S.E. Critchlow, S.H. Teo, A.J. Doherty, A. Priestley, B. Broughton, B. Kysela, H. Beamish, N. Plowman, C.F. Arlett, A.R. Lehmann, S.P. Jackson, P. A. Jeggo, Identification of a defect in DNA ligase IV in a radiosensitive leukaemia patient, Curr. Biol. 9 (1999) 699–702.
[58] E. Riballo, A.J. Doherty, Y. Dai, T. Stiff, M.A. Oettinger, P.A. Jeggo, B. Kysela, Cellular and biochemical impact of a mutation in DNA ligase IV conferring clinical Radiosensitivity*, J. Biol. Chem. 276 (2001) 31124–31132.
[59] J. Smith, E. Riballo, B. Kysela, C. Baldeyron, K. Manolis, C. Masson, M.R. Lieber, D. Papadopoulo, P.J.N.A.R. Jeggo, Impact of DNA Ligase IV on the Fidelity of End Joining in Human Cells 31, 2003, pp. 2157–2167.
[60] N. Adachi, T. Ishino, Y. Ishii, S. Takeda, H. Koyama, DNA ligase IV-deficient cells are more resistant to ionizing radiation in the absence of Ku70: implications for DNA double-strand break repair, Proc. Natl. Acad. Sci. U. S. A. 98 (2001) 12109–12113.
[61] T. Oppliger, F.E. Würgler, C. Sengstag, A plasmid system to monitor gene conversion and reciprocal recombination in vitro, Mutat. Res. 291 (1993) 181–192.
[62] S. Sharma, B. Choudhary, S.C. Raghavan, Efficiency of nonhomologous DNA end joining varies among somatic tissues, despite similarity in mechanism, Cell. Mol. Life Sci. 68 (2011) 661–676.
[63] A.K. Naik, M.R. Lieber, S.C. Raghavan, Cytosines, but not purines, determine recombination activating gene (RAG)-induced breaks on Heteroduplex DNA structures IMPLICATIONS FOR GENOMIC INSTABILITY, J. Biol. Chem. 285 (2010) 7587–7597.
[64] M. Nambiar, S.C. Raghavan, Mechanism of fragility at BCL2 gene minor breakpoint cluster region during t(14;18) chromosomal translocation*, J. Biol. Chem. 287 (2012) 8688–8701.
[65] A.K. Naik, S.C. Raghavan, P1 nuclease cleavage is dependent on length of the mismatches in DNA, DNA Repair (Amst) 7 (2008) 1384–1391.
[66] D. Ghosh, N.M. Nilavar, S.C. Raghavan, A novel KU70-mutant human leukemic cell line generated using CRISPR-Cas9 shows increased sensitivity to DSB inducing agents and reduced NHEJ activity, Biochim. Biophys. Acta Gen. Subj. 1866 (2022), 130246.
[67] R. Kumari, U. Roy, S. Desai, N.M. Nilavar, A. Van Nieuwenhuijze, A. Paranjape, G. Radha, P. Bawa, M. Srivastava, M. Nambiar, K.N. Balaji, A. Liston, B. Choudhary, S.C. Raghavan, MicroRNA miR-29c regulates RAG1 expression and modulates V(D)J recombination during B cell development, Cell Rep. 36 (2021), 109390.
[68] C.V. Kavitha, M. Nambiar, P.B. Narayanaswamy, E. Thomas, U. Rathore, C. S. Ananda Kumar, B. Choudhary, K.S. Rangappa, S.C. Raghavan, Propyl-2-(8-(3,4-difluorobenzyl)-2′,5′-dioxo-8-azaspiro[bicyclo[3.2.1] octane-3,4′-imidazolidine]-1′-yl) acetate induces apoptosis in human leukemia cells through mitochondrial pathway following cell cycle arrest, PLoS One 8 (2013), e69103.
[69] T.S. Kumar, V. Kari, B. Choudhary, M. Nambiar, T.S. Akila, S.C. Raghavan, Anti-apoptotic protein BCL2 Down-regulates DNA end joining in cancer cells, J. BiolChem. 285 (2010) 32657–32670.
[70] R. Sebastian, S.C. Raghavan, Induction of DNA damage and erroneous repair can explain genomic instability caused by endosulfan, Carcinogenesis 37 (2016) 929–940.
[71] C.R. Sathees, M.J. Raman, Mouse testicular extracts process DNA double-strand breaks efficiently by DNA end-to-end joining, Mutat. Res. 433 (1999) 1–13.
[72] K.K. Chiruvella, R. Sebastian, S. Sharma, A.A. Karande, B. Choudhary, S. C. Raghavan, Time-dependent predominance of nonhomologous DNA end-joining pathways during embryonic development in mice, J. Mol. Biol. 417 (2012) 197–211.
[73] P. Baumann, S.C. West, DNA end-joining catalyzed by human cell-free extracts, Proc. Natl. Acad. Sci. U. S. A. 95 (1998) 14066–14070.
[74] S. Dahal, S. Dubey, S.C. Raghavan, Homologous recombination-mediated repair of DNA double-strand breaks operates in mammalian mitochondria, Cell. Mol. Life Sci. 75 (2018) 1641–1655.
[75] N. Bennardo, A. Cheng, N. Huang, J.M. Stark, Alternative-NHEJ is a mechanistically distinct pathway of mammalian chromosome break repair, PLoS Genet. 4 (2008), e1000110.
[76] V. Rawat, G. Bortolussi, S. Gazzin, C. Tiribelli, A.F. Muro, Bilirubin-induced oxidative stress leads to DNA damage in the cerebellum of Hyperbilirubinemic neonatal mice and activates DNA double-Strand break repair pathways in human cells, Oxidative Med. Cell. Longev. 2018 (2018).
[77] V. Gopalakrishnan, S. Dahal, G. Radha, S. Sharma, S.C. Raghavan, B. Choudhary, Characterization of DNA double-strand break repair pathways in diffuse large B cell lymphoma, Mol. Carcinog. 58 (2019) 219–233.
[78] V. Tripathi, H. Agarwal, S. Priya, H. Batra, P. Modi, M. Pandey, D. Saha, S. C. Raghavan, S. Sengupta, MRN complex-dependent recruitment of ubiquitylated BLM helicase to DSBs negatively regulates DNA repair pathways, Nat. Commun. 9 (2018) 1016.
[79] S.C. Raghavan, M.J. Raman, Nonhomologous end joining of complementary and noncomplementary DNA termini in mouse testicular extracts, DNA Repair 3 (2004) 1297–1310.
[80] S. Srivastava, S. Dahal, S.J. Naidu, D. Anand, V. Gopalakrishnan, R. Kooloth Valappil, S.C. Raghavan, DNA double-strand break repair in Penaeus monodon is predominantly dependent on homologous recombination, DNA Res. 24 (2017) 117–128.
[81] J. Sambrook, E.F. Fritsch, T. Maniatis, Molecular Cloning: a Laboratory Manual, Cold spring harbor laboratory press, 1989.
[82] S. Dahal, H. Siddiqua, S. Sharma, R.K. Babu, D. Rathore, S. Sharma, S. C. Raghavan, Unleashing a novel function of endonuclease G in mitochondrial genome instability, Elife 11 (2022).
[83] S.M. Javadekar, N.M. Nilavar, A. Paranjape, K. Das, S.C. Raghavan, Characterization of G-quadruplex antibody reveals differential specificity for G4 DNA forms, DNA Res. 27 (2020).
[84] N. Kumari, S.V. Vartak, S. Dahal, S. Kumari, S.S. Desai, V. Gopalakrishnan, B. Choudhary, S.C. Raghavan, G-quadruplex structures contribute to differential radiosensitivity of the human genome, iScience 21 (2019) 288–307.
[85] S. Al-Nasiry, N. Geusens, M. Hanssens, C. Luyten, R. Pijnenborg, The use of Alamar blue assay for quantitative analysis of viability, migration and invasion of choriocarcinoma cells, Hum. Reprod. 22 (2007) 1304–1309.
[86] U. Ray, S. Sharma, I. Kapoor, S. Kumari, V. Gopalakrishnan, S.V. Vartak, N. Kumari, U. Varshney, S.C. Raghavan, G4 DNA present at human telomeric DNA contributes toward reduced sensitivity to γ-radiation induced oxidative damage, but not bulky adduct formation, Int. J. Radiat. Biol. 97 (2021) 1166–1180.
[87] A.M. Paranjape, S.S. Desai, M. Nishana, U. Roy, N.M. Nilavar, A. Mondal, R. Kumari, G. Radha, V.K. Katapadi, B. Choudhary, S.C. Raghavan, Nonamer dependent RAG cleavage at CpGs can explain mechanism of chromosomal translocations associated to lymphoid cancers, PLoS Genet. 18 (2022), e1010421.
[88] M. Modesti, J.E. Hesse, M. Gellert, DNA binding of Xrcc4 protein is associated with V(D)J recombination but not with stimulation of DNA ligase IV activity, EMBO J. 18 (1999) 2008–2018.
[89] E. Gasteiger, A. Gattiker, C. Hoogland, I. Ivanyi, R.D. Appel, A. Bairoch, ExPASy: the proteomics server for in-depth protein knowledge and analysis, Nucleic Acids Res. 31 (2003) 3784–3788.
[90] H.H.Y. Chang, N.R. Pannunzio, N. Adachi, M.R. Lieber, Non-homologous DNA end joining and alternative pathways to double-strand break repair, Nat. Rev. Mol. Cell Biol. 18 (2017) 495–506.
[91] S. Oh, Y. Wang, J. Zimbric, E.A. Hendrickson, Human LIGIV is synthetically lethal with the loss of Rad54B-dependent recombination and is required for certain chromosome fusion events induced by telomere dysfunction, Nucleic Acids Res. 41 (2012) 1734–1749.
[92] K.M. Frank, N.E. Sharpless, Y. Gao, J.M. Sekiguchi, D.O. Ferguson, C. Zhu, J. P. Manis, J. Horner, R.A. DePinho, F.W. Alt, DNA ligase IV deficiency in mice leads to defective neurogenesis and embryonic lethality via the p53 pathway, Mol. Cell 5 (2000) 993–1002.
[93] J. Smith, E. Riballo, B. Kysela, C. Baldeyron, K. Manolis, C. Masson, M.R. Lieber, D. Papadopoulo, P. Jeggo, Impact of DNA ligase IV on the fidelity of end joining in human cells, Nucleic Acids Res. 31 (2003) 2157–2167.
[94] D.E. Barnes, G. Stamp, I. Rosewell, A. Denzel, T. Lindahl, Targeted disruption of the gene encoding DNA ligase IV leads to lethality in embryonic mice, Curr. Biol. 8 (1998) 1395–1398.
[95] C.J. Norbury, B. Zhivotovsky, DNA damage-induced apoptosis, Oncogene 23 (2004) 2797–2808.
[96] J.Y.J. Wang, DNA damage and apoptosis, Cell Death Differ. 8 (2001) 1047–1048.
[97] N.J. Goff, M. Brenière, C.J. Buehl, A.J. de Melo, H. Huskova, T. Ochi, T. L. Blundell, W. Mao, K. Yu, M. Modesti, K. Meek, Catalytically inactive DNA ligase IV promotes DNA repair in living cells, Nucleic Acids Res. 50 (2022) 11058–11071.
[98] X. Cao, E. Kouyama-Suzuki, B. Pang, T. Kurihara, T. Mori, T. Yanagawa, Y. Shirai, K. Tabuchi, Inhibition of DNA ligase IV enhances the CRISPR/Cas9-mediated knock-in efficiency in mouse brain neurons, Biochem. Biophys. Res. Commun. 533 (2020) 449–457.
[99] D. Yang, M.A. Scavuzzo, J. Chmielowiec, R. Sharp, A. Bajic, M. Borowiak, Enrichment of G2/M cell cycle phase in human pluripotent stem cells enhances HDR-mediated gene repair with customizable endonucleases, Sci. Rep. 6 (2016) 21264.
[100] C. Wang, Z. Sun, M. Wang, Z. Jiang, M. Zhang, H. Cao, L. Luo, C. Qiao, H. Xiao, G. Chen, X. Li, J. Liu, Z. Wei, B. Shen, J. Wang, J. Feng, Novel CRISPR/Cas9-mediated knockout of LIG4 increases efficiency of site-specific integration in Chinese hamster ovary cell line, Biotechnol. Lett. 44 (2022) 1063–1072.
[101] G. Li, X. Zhang, C. Zhong, J. Mo, R. Quan, J. Yang, D. Liu, Z. Li, H. Yang, Z. Wu, Small molecules enhance CRISPR/Cas9-mediated homology-directed genome editing in primary cells, Sci. Rep. 7 (2017) 8943.
[102] T. Maruyama, S.K. Dougan, M.C. Truttmann, A.M. Bilate, J.R. Ingram, H. L. Ploegh, Increasing the efficiency of precise genome editing with CRISPR-Cas9 by inhibition of nonhomologous end joining, Nat. Biotechnol. 33 (2015) 538–542.
[103] K.K. Khanna, S.P. Jackson, DNA double-strand breaks: signaling, repair and the cancer connection, Nat. Genet. 27 (2001) 247–254.
[104] N. Waddell, M. Pajic, A.M. Patch, D.K. Chang, K.S. Kassahn, P. Bailey, A.L. Johns, D. Miller, K. Nones, K. Quek, M.C. Quinn, A.J. Robertson, M.Z. Fadlullah, T. J. Bruxner, A.N. Christ, I. Harliwong, S. Idrisoglu, S. Manning, C. Nourse, E. Nourbakhsh, S. Wani, P.J. Wilson, E. Markham, N. Cloonan, M.J. Anderson, J. L. Fink, O. Holmes, S.H. Kazakoff, C. Leonard, F. Newell, B. Poudel, S. Song, D. Taylor, N. Waddell, S. Wood, Q. Xu, J. Wu, M. Pinese, M.J. Cowley, H.C. Lee, M.D. Jones, A.M. Nagrial, J. Humphris, L.A. Chantrill, V. Chin, A.M. Steinmann, A. Mawson, E.S. Humphrey, E.K. Colvin, A. Chou, C.J. Scarlett, A.V. Pinho, M. Giry-Laterriere, I. Rooman, J.S. Samra, J.G. Kench, J.A. Pettitt, N.D. Merrett,

C. Toon, K. Epari, N.Q. Nguyen, A. Barbour, N. Zeps, N.B. Jamieson, J.S. Graham, S.P. Niclou, R. Bjerkvig, R. Grützmann, D. Aust, R.H. Hruban, A. Maitra, C. A. Iacobuzio-Donahue, C.L. Wolfgang, R.A. Morgan, R.T. Lawlor, V. Corbo, C. Bassi, M. Falconi, G. Zamboni, G. Tortora, M.A. Tempero, A.J. Gill, J. R. Eshleman, C. Pilarsky, A. Scarpa, E.A. Musgrove, J.V. Pearson, A.V. Biankin, S. M. Grimmond, Whole genomes redefine the mutational landscape of pancreatic cancer, Nature 518 (2015) 495–501.

[105] S. Lodovichi, T. Cervelli, A. Pellicioli, A. Galli, Inhibition of DNA repair in Cancer therapy: toward a multi-target approach, Int. J. Mol. Sci. 21 (2020) 6684.

[106] M. Wang, S. Chen, D. Ao, Targeting DNA repair pathway in cancer: mechanisms and clinical application, MedComm 2 (2021) (2020) 654–691.

[107] M. De Palma, D. Hanahan, The biology of personalized cancer medicine: facing individual complexities underlying hallmark capabilities, Mol. Oncol. 6 (2012) 111–127.

[108] Y.T. Lee, Y.J. Tan, C.E. Oon, Molecular targeted therapy: treating cancer with specificity, Eur. J. Pharmacol. 834 (2018) 188–196.